

June 25, 2019

**GMD-2019-15: Revision**

Dear Editor,

We are pleased to submit our revised manuscript entitled: “Developing a monthly radiative kernel for surface albedo change from satellite climatologies of Earth’s shortwave radiation budget: CACK v1.0” for publication consideration in *Geoscientific Model Development*.

Major changes to the manuscript include:

- A major re-structuring to improve overall flow and readability. This re-structuring was necessary to showcase CACK v1.0 as a comprehensive, transparent, and flexible dataset built on a novel model (parameterization) of shortwave radiation transfer.
- An expanded analysis of CACK’s performance including new content on uncertainty and two new demonstrations of its application
- An improved description of the methods to ensure reproducibility, in particular that pertaining to the symbolic regression analysis
- The addition of a Supporting Information document providing additional detail surrounding CACK’s uncertainty calculations, the symbolic regression method and results, and a detailed description of the CACK v1.0 dataset which now includes estimates for three sources of uncertainty.

The revised manuscript has increased by ~2,000 words, 3 figures, and 1 table. We feel confident that our revisions go above and beyond that which is required to satisfy reviewers and add notable value to the paper serving to elevate its overall impact. For instance, the new and comprehensive analysis on uncertainty and its inclusion in CACK v1.0 should make it more attractive as a credible candidate for use as part of a future Monitoring, Reporting, and Verification (MRV) framework for radiative forcing impacts of albedo changes on land.

Please do not hesitate contacting us should you require additional information or clarification.

Kind Regards,

Ryan M. Bright and Tom L. O’Halloran

## Reponses to Anonymous Referee #1

This study by Bright and O'Halloran developed shortwave radiative kernels based on the CERES EBAF products, which would be an alternative to GCM-based kernels. The performance of the observation-based kernels is also evaluated based on the multi-GCM mean. This is an interesting study, and the developed shortwave radiative kernels have the potential of being used for land use-climate studies. However, I think the manuscript needs some improvement and further development in the analysis before it can be published.

We thank Anonymous Referee #1 for his/her constructive feedback. To address his/her major concerns, we have provided more detail about the GCM kernels and their uncertainties, improved the description of our methodology, and provided two examples illustrating CACK's application.

My major concerns include:

1. The evaluation of CERES kernels uses four GCM kernels as benchmarks. I am wondering the uncertainties among the different GCMs. **GCM uncertainties are largely related to their representation of low-level cloud cover and properties** (please see our reference to Dolinar *et al.* 2015 [original manuscript P3 L67]). Regarding cloud properties, one of the major differences among GCMs is related to the representation of atmospheric liquid water/ice associated with convective clouds. Of the four GCMs we considered, only CAM5 and GFDL attempt to model the effects of precipitating and/or convective core ice and liquid in their radiation calculations. We add this detail in (new) Section 2.a and provide a new citation (e.g., to Li *et al.* (2013)). First, why are these four models chosen? These GCM kernels were chosen simply because at the time the study commenced these were the only ones available. We add this rationale to the main text (new Section 2.a). But why CAM3 and GFDL are not mentioned in the results? We carried out a two-stage evaluation, where CAM3 and GFDL comprised part of the “multi-GCM mean” benchmark we used in the first stage (described in new Section 4a), whose results are presented in (new) Section 5, Figures 1 & 2. We hope our re-organization and improved methods descriptions have now made this clearer. Second, for Figure 1, if plotting the radiative kernel for individual GCMs, is there a large spread like the CERES-based estimates? This is a great question and we agree that the spread in GCMs should be made more visible. We have revised Figure 1 such that it now shows the spread (taken as 1 standard deviation) in latitudinal means across the four GCMs. Third, are the author's conclusions model-dependent? Because the BO18 kernel is trained using the multi-GCM mean as the reference, it is not surprising that it has better performance than other CERES kernels. This is a fair comment and valid concern. To check this, we re-ran the machine learning algorithm twice, first using a random sample of the CAM5 kernel (as the dependent) with its own boundary fluxes (as independents), the second time using a random sample of the ECHAM6 kernel with its own boundary fluxes as input (note: these were the only two kernels for which the boundary fluxes used to derive them were also available to us). The BO18 model emerged as the best solution (i.e., model form) common to the two independent machine learning analyses. Because the BO18 model was then applied using CERES EBAF inputs and subsequently compared to a multi-GCM mean that included the two additional GCM kernels (i.e., GFDL and CAM3) that were not part of the model training exercise, we feel confident that the BO18 model is robust and insensitive to the GCM kernels used for training. However, if using a single GCM (or including other GCMs, like HadGEM2 radiative kernels, Smith 2018) as the benchmarks, will QH06 or ANISO still be better than other kernel models? Yes, we indeed found this to be the case – that whether benchmarking to multi-GCM means or to specific GCMs, the CERES kernel performance ranking remained unchanged (excluding the QH06 kernel for the reason provided in revised Section 5b). The authors may

need more analysis and discussion about the model dependency. We have added a section in the Discussion regarding BO18's model (in)dependency.

2. One of the motivations of this study is “atmospheric state variables used as model input are limited to single years, thus being sensitive to anomalous weather conditions that may have occurred in those years”. Can you explain more about this? As the authors mentioned in L278, they are comparing the multi-year CERES kernel to a single-year GCM kernel. I assume the GCM simulations are only one-year long? The authors may need to provide more description and discussion about these GCM simulations. The GCM simulations from which the kernels are derived are indeed carried out for a period of one year. However, when going back to double check this, we discovered that we had mistook this for the temporal signature and duration of the prescribed atmospheric background state, which for three of the four GCM kernels does extend beyond a single year. We now include a new table (Table 1) that summarizes this and other differences between the GCMs used to derive the GCM kernels and delete the incorrect statement quoted above. If the simulates are for a specific year (which year?), or a climatological run, are they comparable to the CERES-based kernel models which are for the period 2001-2016. No GCM kernel is comparable to the 2001-2016 CERES kernel; background climatologies of ECHAM6, CAM3, and GFDL kernels span several years (or decades) but all pre-date the CERES EBAF era. CAM5's background does fall within the CERES era but is based on a single year only. These discrepancies are why we chose to compare to the mean of all four kernels in our initial performance screening. We chose not to compare the CAM5 kernel to a CERES kernel based on the same background year because the atmospheric state information underlying CAM5 is not based on CERES EBAF (i.e., it would still not be possible to attribute disagreement to differences in the representation of shortwave radiative transfer). This is why we chose instead to emulate CAM5 with the BO18 parameterization run with CAM5's own boundary fluxes. Additionally, I am curious about the inter-annual variability of the multi-year CERES kernels. The interannual variability of a kernel based on CERES can now be inferred from the results of our second application example (Figure 7 C, southern Amazonian deforestation).

3. This study is started with the “need within LULCC science community for simple and transparent tools for predicting radiative forcings from surface albedo changes”. Is it possible to provide a simple example of how to apply CACK v1.0 to the LULCC studies? This is a fair request and have thus invested notable effort into demonstrating how both a climatological CACK and a temporally-explicit CACK may be applied to estimate radiative forcings in LULCC studies (New Sections 4 d & e, 5 d & e, and new Figures 6 & 7).

Specific comments:

1. The organization of section 2 and section 3 is a little confusing. The title of section 2 is “Review of existing approaches”, but most of the kernels described in section 3 are also “existing approaches”, aren't they? We fully agree and have carried out a major re-organization of the manuscript. We are confident that the new manuscript structure is more intuitive and easier to follow and digest.

2. L40, What do you mean by “offline”? Run land surface model offline? Here we mean that GCMs are not practical to apply for estimating albedo change RFs for single locations, and that other modeling approaches have been applied for this purpose involving stand-alone radiative transfer modeling in which the surface and atmosphere are not coupled. I also can't find the paper (Randerson et al. 2006) in the reference. Thank you for pointing out this missing reference which has now been added.

3. L151, Eq. (3) and Eq. (4), are \_\_s and \_\_ the same thing? If yes, it would be better to keep the consistency. **Yes, these are the same and have been corrected (thanks).**

4. L247, Which part (or period) of data is used for model training, and which part is used for prediction? **Model training and prediction datasets are based on a random sampling in both time and space (200,000 grid cells in each).** This detail has been added to (new) Section 3 d).

5. L263, It should be “e. Initial screening of candidate models for a CERES-based kernel”. **Corrected.**

6. L409, They are mean absolute bias, not RMSD. **Corrected.**

7. L441-444, Can the authors explain more about how the land-based solar radiation management is an example of the CACK’s flexibility? **This was a poorly constructed sentence which has been deleted in the revision.**

Reference:

Smith, Christopher J. (2018) HadGEM2 radiative kernels. University of Leeds.  
[Dataset] <https://doi.org/10.5518/406>

## Responses to Anonymous Referee #2

### General comments

The manuscript presented by Bright and O’Halloran suggests the use of a new kernel (CACKv1.0) to derive radiative forcing at the top of the atmosphere from surface albedo changes. This kernel is derived by applying a machine learning technique to identify a formula which can best reproduce the results from kernels derived from Global Circulation Models, once it is applied to CERES satellite-derived data. The authors argue that compared to GCM-derived kernels, this new formula would 1) enable a more transparent derivation of radiative forcing from surface albedo changes, and 2) rely on data from several years. Their analysis shows that the new formula performs better at mimicking the results from GCM-derived kernels compared to previously suggested formulations. They suggest the use of their results by the scientists studying the impacts of land-use and land-cover changes (LULCC) on climate to improve their calculations of radiative forcing from surface albedo changes.

Having an easily applicable kernel that reproduces the results from GCMs can indeed be useful for the LULCC community, and in that sense the authors’ initiative is welcome and scientifically significant. Having said that, there are a couple of issues with the authors’ approach, while the methodology could be better described to ensure reproducibility of the results. Overall, substantial work also needs to be done on the writing to improve understandability of the manuscript. These issues are not insurmountable, but I recommend that they are addressed before the manuscript is accepted.

We thank Anonymous Referee #2 for his/her constructive feedback. To address his/her major concerns, we have carried out a major re-structuring of the paper that we now believe is easier to follow and more intuitive to digest. This includes more attention to CACK’s uncertainties as well as the uncertainties between GCM kernels, and we now include uncertainty estimates for CACK in effort to make CACK v1.0 a more attractive and complete dataset. Lastly, we have also

invested notable effort to improve the description of our methods to better-ensure reproducibility of results.

- Specific comments

The real added value of CACK compared to previously suggested simple formulations can only be assessed in light of the uncertainties between GCM kernels. These thus need to be included at least in Figure 1 and discussed in the manuscript, so that the readers can assess for themselves how much of a difference using CACK rather than a simple isotropic kernel (for example) makes. This is a fair comment. We have added additional text describing major sources of uncertainty in GCM-based kernels (new Section 2.a), a new table (new Table 1) highlighting the major differences between them, and a new Figure 1 that now shows the spread among the four GCM kernels we employed (expressed in terms of the seasonal and latitude band mean standard deviations). The authors also mention that the GCM-derived kernels are based on single years of forcing data. This renders them uncertain and thus less appropriate as a benchmark, therefore the authors choose to use the multi-GCM mean kernel as a reference to partly alleviate the lack of consideration of interannual variability when they were derived. This seems reasonable but only

partly alleviates the issue. In addition to being explicitly shown and discussed, the uncertainties about GCM-derived kernels (both related to model spread and interannual variability) need to be acknowledged in the Discussion. Even in the current state, more conclusions could be drawn from Figure 1 by describing for example which kernels perform worst against the GCM-derived ones and potentially advancing reasons why this is the case. We believe the revised Figure 1 sufficiently demonstrates the performance of all CERES kernel candidates in light of discrepancies among the GCM kernels themselves.

The methodology should be more detailed to be able to understand how Equation 16 is derived. Which optimal structures and coefficients are considered during the symbolic regression? What should make the reader think that this approach doesn't miss potentially relevant formulas? And which "boundary fluxes (or system parameters derived from these fluxes) that minimized the sum of squared residuals. . ." were considered? This information should at least be provided in the Supplementary Material. This is a fair comment and have thus provided more detail surrounding Eq. (16) (now Eq. (17)) in (new) Section 2.d, including what fluxes were included and what constraints were applied, as well as providing other detail in a new section of the Supporting Information. In the Supporting Information we provide examples of alternate model structures obtained from the machine learning exercise, their performance metrics, and the criteria we applied in the model selection process.

It is also not so clear from the current manuscript why certain choices were made regarding the GCM and kernel selections. Why are four GCM kernels included in the study, are these the only ones available? Correct, these are the only four GCM kernels available at the time the study commenced. We add this rationale to the main text (new Section 2 a). Is there some information existing on the quality of these kernels that guided the selection? Could the authors justify why they "emulated" the kernels of just two GCMs in a second step? Only ECHAM6 and CAM5 kernels were used in the emulation exercise because these were the only two kernels for which the boundary fluxes were also provided (which were needed for the machine learning-based model selection and for kernel emulation). We add this justification to (new) Section 3 b. It seems like only the 3 kernels performing best against the GCM-derived ones were retained for further analysis, but this is also not explicitly mentioned. We have added a sentence at the end of

(new) Section 4 a explicitly stating why only these three kernels were retained for further analysis (i.e., they were the top performers of the initial CERES candidate model evaluation exercise).

The structure of the manuscript could be improved to facilitate understandability. For example, why not mentioning the isotropic and anisotropic kernels, as well as the kernel from Qu and Hall in Section 2 already. Currently, at first it may read like they have been derived by the authors. The names of the studies that introduced other types of statistical kernels could also be added in the subsection titles to help the reader follow. **We agree that our manuscript needed a more logical organization to facilitate improved readability.** We believe the new organization leaves the reader with zero doubt about the origin of the CERES model candidates we consider in the paper.

The description of the CERES dataset also seems misplaced in Section 2. Additionally, in some occurrences the subsection numbering is wrong and the placeholders for Figures or Tables misplaced. **We agree and have re-structured the manuscript accordingly such that description of the CERES EBAF v4 products is now provided up front in the Introduction.** We have checked and updated all section/table/figure numbering.

Last but not least, the CACK dataset is only mentioned in the conclusion, although from the title it sounds like an important output of the study. If this is the case, it would need to be introduced in the abstract and the introduction of the manuscript. But ultimately, one may wonder whether describing CACK as a dataset is appropriate. Could the authors maybe develop on what makes it more than just applying Eq. 16 to CERES data, for example in terms of pre-processing or perspectives for updates, etc.? **We agree that the value of CACK v1.0 packaged as a dataset (i.e., more than just Eq. (17) applied to CERES data) ought to be highlighted and clearly showcased.** We have therefore invested considerable effort into describing and quantifying the various sources of uncertainty of CACK and include these as part of a more comprehensive CACK v1.0 data product. We believe this addition strengthens the credibility of CACK v1.0 as a data product and as a viable tool for the advancement of a verification framework for biogeophysical climate forcings on land.

- Technical comments

- l. 68: “An additional downside is the that”. Check typo **Corrected typo**.
- l. 157: to facilitate understandability it could be good to repeat the downsides of GCMderived kernels here **We agree and include this as part of (new) Section 2 a.**
- l. 425: “course” should read “coarse” **Corrected**.
- l. 704-705: can the authors make clearer what is meant by “100X100 sample grid”? **Clarified**.

1 **Developing a monthly [albedo change](#)-radiative [forcing](#) kernel for surface albedo change**  
2 **from satellite climatologies of Earth's shortwave radiation budget: CACK v1.0**

3

4 Ryan M. Bright<sup>1\*</sup> and Thomas L. O'Halloran<sup>2,3</sup>

5

6 1 – Norwegian Institute of Bioeconomy Research, Ås, Norway

7 2 – Department of Forestry and Environmental Conservation, Clemson University, Clemson,  
8 South Carolina, USA.

9 3 – Baruch Institute of Coastal Ecology and Forest Science, Clemson University,  
10 Georgetown, South Carolina, USA

11 \*Contact: [ryan.bright@nibio.no](mailto:ryan.bright@nibio.no)

12

13 **Abstract**

14 Due to the potential for land use / land cover change (LULCC) to alter surface albedo, there is  
15 need within the LULCC science community for simple and transparent tools for predicting  
16 radiative forcings ( $\Delta F$ ) from surface albedo changes ( $\Delta \alpha_s$ ). To that end, the radiative kernel  
17 technique – developed by the climate modeling community to diagnose internal feedbacks  
18 within general circulation models (GCMs) – has been adopted by the LULCC science  
19 community as a tool to perform offline  $\Delta F$  calculations for  $\Delta \alpha_s$ . However, the [codes and](#)  
20 [data behind the GCM kernels are not readily transparent, and the climatologies of the](#)  
21 [atmospheric state variables used to derive them GCM vary widely both in time period and](#)  
22 [duration. Codes are not readily transparent and the atmospheric state variables used as model](#)  
23 [input are limited to single years, thus being sensitive to anomalous weather conditions that](#)  
24 [may have occurred in those simulated years.](#) Observation-based kernels [founded on longer-](#)  
25 [term climatologies of Earth's atmospheric state](#) offer an attractive alternative to GCM-based

26 kernels and could be updated annually at relatively low costs. Here, [we present a radiative](#)  
27 [kernel for surface albedo change](#) [we evaluate](#) [founded on simplified models](#) [a novel, simplified](#)  
28 [parameterization](#) [of shortwave radiative transfer](#) [as candidates for an albedo change kernel](#)  
29 [founded on](#) [driven with inputs from the](#) [Clouds and the Earth's Radiant Energy System](#)  
30 (CERES) Energy Balance and Filled (EBAF) products. [When based on a 16-year climatology](#)  
31 [\(2001-2016\), we find that the CERES albedo change kernel – or CACK –](#) [We find that a new,](#)  
32 [simple model supported by statistical analyses gives remarkable agreement when](#)  
33 [benchmarked to](#) [agrees remarkably well with](#) [the mean kernel of four GCMs \(rRMSE =](#)  
34 [14%\)](#) [kernels.](#) [When the novel parameterization underlying CACK is applied to emulate two](#)  
35 [of the GCM kernels using their own boundary fluxes as input, we find even greater agreement](#)  
36 [\(mean rRMSE = 7.4%\), suggesting that this simple and transparent parameterization](#)  
37 [represents a credible candidate for a satellite-based alternative to GCM kernels and to two](#)  
38 [GCM kernels following emulation with their own boundary fluxes as input.](#) [Our findings](#)  
39 [lend support to its candidacy as a satellite based alternative to GCM kernels and to its](#)  
40 [application in land climate studies.](#) [We document and compute the various sources of](#)  
41 [uncertainty underlying CACK and include them as part of a more extensive dataset \(CACK](#)  
42 [v1.0\) while providing examples showcasing its application.](#)

43 **Keywords:** GCM, radiative forcing, land use change, land cover change, LULCC

44

## 45 1. Introduction

46 Diagnosing changes to the shortwave radiation balance at the top-of-the-atmosphere (TOA)  
47 resulting from changes to albedo at the surface ( $\Delta\alpha_s$ ) is an important step in predicting  
48 climate change. However, outside the climate science community, many researchers do not  
49 have the tools to convert  $\Delta\alpha$  to the climate-relevant  $\Delta F$  measure (Bright, 2015; Jones et al.,  
50 2015), which requires a detailed representation of the atmospheric constituents that absorb or

51 scatter solar radiation (e.g. cloud, aerosols, and gases) and a sophisticated radiative transfer  
52 code. For single points in space or for small regions, these calculations are typically  
53 performed offline – meaning without feedbacks to the atmosphere (e.g., [Randerson et al.](#)  
54 [2006](#)(Randerson et al., 2006))). Large-scale investigations (e.g. Amazonian or pan-boreal  
55 LULCC (Dickinson and Henderson-Sellers, 1988;Bonan et al., 1992)) typically prescribe the  
56 land surface layer in a GCM with initial and perturbed states, allowing the radiative transfer  
57 code to interact with the rest of the model. While this has the benefit of allowing interaction  
58 and feedbacks between surface albedo and scattering or absorbing components of the model,  
59 such an approach is computationally expensive and thereby restricts the number of LULCC  
60 scenarios that can be investigated (Atwood et al., 2016). Consequently, this method does not  
61 meet the needs of some modern LULCC studies which may require millions of individual  
62 land cover transitions to be evaluated cost effectively (Lutz and Howarth, 2015;Ghimire et al.,  
63 2014).

64

65 Within the LULCC science community, two methods have primarily met the need for  
66 efficient  $\Delta F$  calculations from  $\Delta\alpha_s$ : simplified parameterizations of atmospheric transfer of  
67 shortwave radiation (Bright and Kvælevåg, 2013;Cherubini et al., 2012;Bozzi et al.,  
68 2015;Muñoz et al., 2010;Caiazzo et al., 2014;Carrer et al., 2018), and radiative kernels  
69 (Ghimire et al., 2014;O'Halloran et al., 2012;Vanderhoof et al., 2013) derived from  
70 sophisticated radiative transfer schemes embedded in GCMs (Soden et al., 2008;Shell et al.,  
71 2008;Pendergrass et al., 2018;Block and Mauritsen, 2014). Simplified parameterizations of  
72 the LULCC science community have not been evaluated comprehensively in space and time.  
73 Bright & Kvælevåg (2013) evaluated the shortwave  $\Delta F$  parameterization of Cherubini *et al.*  
74 (2012) when applied at several [sites distributed](#)–globally [distributed sites](#) on land, finding

75 inconsistencies in performance at individual sites despite good overall cross-site performance.  
76 Radiative kernels (Soden et al., 2008;Shell et al., 2008;Pendergrass et al., 2018;Block and  
77 Mauritsen, 2014) – while being based on state-of-the-art models of radiative transfer – have  
78 the downside of being model-dependent and not readily transparent. While the radiative  
79 transfer codes behind them are well-documented, the scattering components (i.e. aerosols,  
80 gases, and clouds) affecting transmission have many simplifying parameterizations, vary  
81 widely across models, and may contain significant biases (Dolinar et al., 2015;Wang and Su,  
82 2013). An additional downside is ~~the~~ that the atmospheric state climatologies used to  
83 compute the GCM kernels vary widely in their time periods (i.e., from pre-industrial to the  
84 year 2007) and extends durations (from 1 to 1,000 yrs). variables used as model input are  
85 limited to single years, thus being sensitive to anomalous weather conditions that may have  
86 occurred in those years. Further, the application of a state-dependent GCM kernel that is  
87 outdated may be undesirable in regions undergoing rapid changes in cloud cover or aerosol  
88 optical depth, such as in the northwest United States (Free and Sun, 2014) and in southern and  
89 eastern Asia (Zhao et al., 2018;Srivastava, 2017), respectively. An albedo change -kernel  
90 based on Earth-orbiting satellite products remotely sensed observations could be updated  
91 annually to capture changes in atmospheric state at relatively low costs.

92 The NASA Clouds and the Earth's Radiant Energy System (CERES) Energy Balance and  
93 Filled (EBAF) products (CERES Science Team, 2018a, b), which are based largely on  
94 satellite optical remote sensing, provide the monthly mean boundary fluxes and other  
95 atmospheric state information (e.g., cloud area fraction, cloud optical depth) that could be  
96 used to develop a more empirically-based alternative to the GCM-based kernels. The latest  
97 EBAF-TOA Ed4.0 (version 4.0) products have many improvements with respect to the  
98 previous version (version 2.8, Loeb et al. 2009), including the use of advanced and more

99 [consistent input data, retrieval of cloud properties, and instrument calibration \(Kato et al.,](#)  
100 [2018;Loeb et al., 2017\)](#)

101 [Here, we present an albedo change kernel based on the CERES EBAF v4 products – or](#)  
102 [CACK. Underlying CACK is a simplified model of shortwave radiative transfer through a](#)  
103 [one-layer atmosphere. The model form \(or parameterization\) is selected after a two-stage](#)  
104 [performance evaluation of six model candidates: two analytical, one semi-empirical, and](#)  
105 [three empirical. An initial performance screening is implemented where all six model](#)  
106 [candidates are driven with a 16-year climatology \(January 2001 – December 2016\) of](#)  
107 [monthly all-sky boundary fluxes from CERES, with the resulting kernels benchmarked both](#)  
108 [qualitatively and quantitatively against the mean of four GCM-based kernels \(Shell et al.,](#)  
109 [2008;Soden et al., 2008;Pendergrass et al., 2018;Block and Mauritsen, 2014\). Top model](#)  
110 [candidates from the initial performance screening are then subjected to an additional](#)  
111 [performance evaluation where they are applied to emulate two GCM kernels using their own](#)  
112 [boundary fluxes as input, which eliminates possible biases related to differences in the GCM](#)  
113 [representation of clouds or other atmosphere state variables.](#)

114 [We start in Section 2 by providing a brief overview of existing approaches applied in LULCC](#)  
115 [climate studies for estimating  \$\Delta F\$  from  \$\Delta a\$ . We then present the six model candidates in](#)  
116 [Section 3. Section 4 describes the model evaluation and uncertainty quantification methods,](#)  
117 [in addition to two application examples. Results are presented in Section 5, while Section 6](#)  
118 [discusses the merits and uncertainties of a CERES-based kernel relative to GCM-based](#)  
119 [kernels.](#)

120  
121 [Within the atmospheric science community, simplified radiative transfer frameworks have](#)  
122 [been developed, either to diagnose effective surface and atmospheric optical properties from](#)

123 climate model outputs, or to study the relative contributions of changes to these properties on  
124 shortwave flux changes at the top and bottom of the atmosphere (Rasool and Schneider,  
125 1971; Winton, 2005; Winton, 2006; Taylor et al., 2007; Donohoe and Battisti, 2011; Atwood et  
126 al., 2016; Kashimura et al., 2017; Qu and Hall, 2006). These frameworks differ by whether or  
127 not the reflection and transmission properties of the atmospheric layer are assumed to have a  
128 directional dependency (Stephens et al., 2015) and by the number of variables required as  
129 input (Qu and Hall, 2006). Winton (2005) presented a four parameter optical model to  
130 account for the directional dependency of up- and downwelling shortwave fluxes through a  
131 one layer atmosphere and found good agreement (RMSE < 2% globally) when benchmarked  
132 to online radiative transfer calculations. Also considering a directional dependency of the  
133 atmospheric optical properties, Taylor et al. (2007) presented a two parameter model where  
134 atmospheric absorption was assumed to occur at a level above atmospheric reflection.  
135 Donohoe and Battisti (2011) subsequently relaxed the directional dependency assumption and  
136 found the atmospheric attenuation of the surface albedo contribution to planetary albedo to be  
137 8% higher than the model of Taylor et al. (2007). Elsewhere, Qu & Hall (2006) developed a  
138 framework making use of additional known atmospheric properties such as cloud cover  
139 fraction, cloud optical thickness, and the clear sky planetary albedo which proved highly  
140 accurate when model estimates of planetary albedo were evaluated against climate models  
141 and satellite-based datasets.

142 Here, our primary research objective is to thoroughly evaluate a variety of shortwave kernels  
143 derived both analytically and statistically from satellite based climatologies of Earth's  
144 shortwave radiation budget. To this end, we employ a 16 yr. time series of Earth's monthly  
145 mean radiation budget at both TOA (Leeb et al., 2017) and at the surface (Kato et al., 2012)  
146 as input to simplified models linking  $\Delta\alpha_s$  to changes in the outgoing shortwave radiation flux  
147 at TOA. An initial performance screening is implemented where the six observation driven

148 kernels are first assessed both qualitatively and quantitatively against the mean of four GCM  
149 kernels (Shell et al., 2008; Soden et al., 2008; Pendergrass et al., 2018; Block and Mauritsen,  
150 2014). Top performers are then subjected to a more rigorous evaluation where they are  
151 applied to emulate the GCM kernels using the GCM's own boundary fluxes as input, which  
152 eliminates any bias related to differences in the GCM representation of clouds or other  
153 atmosphere state variables. Our results elucidate the merits and uncertainties of empirical  
154 alternatives to those based on GCMs.

155

156 We start in Section 2 by introducing the satellite based energy balance product and the  
157 variables derived from them utilized in this study. We then provide a brief overview of the  
158 GCM based kernels and of the methods currently being applied within the LULCC science  
159 community to estimate instantaneous radiative forcings from surface albedo change. Section  
160 3 details the methods applied to derive candidate GCM kernel alternatives from the radiative  
161 fluxes at Earth's upper and lower boundaries. We then present results of a comparative  
162 analysis in Section 4 and conclude with a brief discussion surrounding the merits and  
163 uncertainties of albedo change kernels based on satellite remote sensing.

164

## 165 2 Review of existing approaches

### 166 *a. Shortwave $\Delta F$ from $\Delta\alpha_s$*

167 Earth's energy balance (at TOA) in an equilibrium state can be written:

$$168 0 = F = LW_{\uparrow}^{TOA} - (SW_{\downarrow}^{TOA} - SW_{\uparrow}^{TOA}) \quad (1)$$

169 where the equilibrium flux  $F$  is a balance between the net solar energy inputs ( $SW_{\downarrow}^{TOA} - SW_{\uparrow}^{TOA}$ )  
 170 and thermal energy output ( $LW_{\uparrow}^{TOA}$ ). Perturbing this balance results in a radiative forcing  
 171  $\Delta F$ , while perturbing the shortwave component is referred to as a shortwave radiative forcing  
 172 and may be written as:

$$173 \Delta F = \Delta(SW_{\downarrow}^{TOA} - SW_{\uparrow}^{TOA}) = \Delta SW_{\downarrow}^{TOA} \left(1 - \frac{SW_{\uparrow}^{TOA}}{SW_{\downarrow}^{TOA}}\right) - SW_{\downarrow}^{TOA} \left(\Delta \frac{SW_{\uparrow}^{TOA}}{SW_{\downarrow}^{TOA}}\right) \quad (2)$$

174 where the shortwave radiative forcing results either from changes to solar energy inputs ( $\Delta SW_{\downarrow}^{TOA}$ ) or from internal perturbations- within the Earth system ( $\Delta \frac{SW_{\uparrow}^{TOA}}{SW_{\downarrow}^{TOA}}$ ). The latter can  
 175 be brought about by changes to the reflective properties of Earth's surface and/or atmosphere  
 176 which is the focus ~~is~~ of this paper.

178 *a. GCM-based radiative kernels*

179 The radiative kernel technique was developed as a way to assess various climate feedbacks  
 180 from climate change simulations across multiple climate models in a computationally efficient  
 181 manner (Shell et al., 2008; Soden et al., 2008). A radiative kernel is defined as the differential  
 182 response of an outgoing radiation flux at TOA to an incremental change in some climate state  
 183 variable -- such as water vapor, air temperature, or surface albedo (Soden et al., 2008). To  
 184 generate a radiative kernel for a change in surface albedo with a GCM, the prescribed surface  
 185 albedo change is perturbed incrementally by 1%, and the response by the outgoing shortwave  
 186 radiation flux at TOA is recorded:

$$187 \Delta SW_{\uparrow}^{TOA} = SW_{\uparrow}^{TOA}(\alpha_s + \Delta \alpha_s) - SW_{\uparrow}^{TOA}(\alpha_s) = \frac{\partial SW_{\uparrow}^{TOA}}{\partial \alpha_s} \Delta \alpha_s \equiv K_{\alpha_s} \Delta \alpha_s \quad (3)$$

Field Code Changed

188 where  $SW_{\uparrow}^{TOA}$  is the outgoing shortwave flux at TOA and  $K_{\alpha_s}$  is the radiative kernel (in  $\text{Wm}^{-2}$ )

Field Code Changed

Field Code Changed

189 <sup>2)</sup> which The NASA Clouds and the Earth's Radiant Energy System (CERES) Energy  
190 Balance and Filled (EBAF) products provide the monthly mean boundary fluxes and  
191 atmospheric state information necessary to derive our GCM kernel alternatives (CERES  
192 Science Team, 2018a, b). The latest EBAF TOA Ed4.0 (version 4.0) products have many  
193 improvements with respect to the previous version (version 2.8, Loeb et al. 2009), including  
194 the use of advanced and more consistent input data, retrieval of cloud properties, and  
195 instrument calibration (Loeb et al. 2018). The temporal extent of the EBAF dataset employed  
196 in our analysis spans the sixteen full calendar years from January 1, 2001 to December 31,  
197 2016 (retrieved April, 2018). An overview of all CERES inputs used in our analysis is  
198 presented in Table 1.

199

200 <Table 1>

201 *a. Shortwave  $\Delta F$  from  $\Delta \alpha_s$*

202 Earth's energy balance (at TOA) in an equilibrium state can be written:

203 
$$0 = F = LW_{\uparrow}^{TOA} - (SW_{\downarrow}^{TOA} - SW_{\uparrow}^{TOA}) \quad (1)$$

204 where the equilibrium flux  $F$  is a balance between the net solar energy inputs ( $SW_{\downarrow}^{TOA} - SW_{\uparrow}^{TOA}$ )  
205 and thermal energy output ( $LW_{\uparrow}^{TOA}$ ). Perturbing this balance results in a radiative forcing  
206  $\Delta F$ , while perturbing the shortwave component is referred to as a shortwave radiative forcing  
207 and may be written as:

208 
$$\Delta F = \Delta(SW_{\downarrow}^{TOA} - SW_{\uparrow}^{TOA}) = \Delta SW_{\downarrow}^{TOA} \left( 1 - \frac{SW_{\uparrow}^{TOA}}{SW_{\downarrow}^{TOA}} \right) - SW_{\downarrow}^{TOA} \left( \Delta \frac{SW_{\uparrow}^{TOA}}{SW_{\downarrow}^{TOA}} \right) \quad (2)$$

210 where the shortwave radiative forcing results either from changes to solar energy inputs (  
211  $\Delta SW_{\downarrow}^{TOA}$ ) or from internal perturbations within the Earth system ( $\Delta \frac{SW_{\uparrow}^{TOA}}{SW_{\downarrow}^{TOA}}$ ). The latter can  
212 be brought about by changes to the reflective properties of Earth's surface and/or atmosphere  
213 which is the focus in this paper.

214 *b. GCM-based radiative kernels*

215 The radiative kernel technique was developed as a way to assess various climate feedbacks  
216 from climate change simulations across multiple climate models in a computationally efficient  
217 manner (Shell et al., 2008; Soden et al., 2008). A radiative kernel is defined as the differential  
218 response of an outgoing radiation flux at TOA to an incremental change in some climate  
219 feedback variable such as water vapor, air temperature, or surface albedo (Soden et al.,  
220 2008). To generate a radiative kernel for a change in surface albedo  $\Delta\alpha$  with a GCM, the  
221 prescribed surface albedo is perturbed incrementally by 1% and the response by  $SW_{\uparrow}^{TOA}$  is  
222 recorded, which can be expressed as:

$$223 \Delta SW_{\uparrow}^{TOA} = SW_{\uparrow}^{TOA}(\alpha_s + \Delta\alpha_s) - SW_{\uparrow}^{TOA}(\alpha_s) = \frac{\partial SW_{\uparrow}^{TOA}}{\partial \alpha_s} \Delta\alpha_s = K_{\alpha} \Delta\alpha_s \quad (3)$$

224 where  $K_{\alpha}$  is the radiative kernel (in  $\text{W m}^{-2}$ ). The albedo change kernel can then be used  
225 with Eq. (1) to estimate an instantaneous shortwave radiative forcing ( $\Delta F$ ) at TOA:

$$226 F + \Delta F = LW_{\uparrow}^{TOA} - (SW_{\downarrow}^{TOA} - SW_{\uparrow}^{TOA} + K_{\alpha} \Delta\alpha_s) \quad (4)$$
$$\Delta F = -K_{\alpha} \Delta\alpha_s$$

227 To the best of our knowledge, four albedo change kernels have been developed based on the  
228 following GCMs: the Community Atmosphere Model version 3, or CAM3 (Shell et al.,  
229 2008), the Community Atmosphere Model version 5, or CAM5 (Pendergrass et al., 2018), the  
230 European Center and Hamburg model version 6, or ECHAM6 (Block and Mauritsen, 2014),  
231 and the Geophysical Fluid Dynamics Laboratory model version AM2p12b, or GFDL (Soden

232 et al., 2008). These four GCM kernels vary in their vertical and horizontal resolutions, their  
233 parameterizations of shortwave radiative transfer, and their prescribed atmospheric state  
234 climatologies. (Søden et al., 2008;Shell et al., 2008;Block and Mauritsen, 2014;Pendergrass  
235 et al., 2018)These differences are summarized in Table 1. Apart from differences in their  
236 prescribed atmospheric background states and radiative transfer schemes, a major source of  
237 uncertainty in GCM-based kernels is related to the GCM representation of atmospheric liquid  
238 water/ice associated with convective clouds; of the four aforementioned GCMs, only CAM5  
239 and GFDL attempt to model the effects of convective core ice and liquid in their radiation  
240 calculations (Li et al., 2013).

241

242 <Table 1>

243

244 *b. Single-layer atmosphere models of shortwave radiation transfer*

245 Within the atmospheric science community, various simplified analytical or semi-empirical  
246 modeling frameworks have been developed, either to diagnose effective surface and  
247 atmospheric optical properties from climate model outputs, or to study the relative  
248 contributions of changes to these properties on shortwave flux changes at the top and bottom  
249 of the atmosphere (Rasool and Schneider, 1971;Winton, 2005;Winton, 2006;Taylor et al.,  
250 2007;Donohoe and Battisti, 2011;Atwood et al., 2016;Kashimura et al., 2017;Qu and Hall,  
251 2006). While these frameworks all treat the atmosphere as a single layer, they differ by  
252 whether or not the reflection and transmission properties of this layer are assumed to have a  
253 directional dependency (Stephens et al., 2015) and by whether or not inputs other than those  
254 derived from the boundary fluxes are required (e.g. cloud properties; (Qu and Hall, 2006)).

255 Winton (2005) presented a semi-empirical four-parameter optical model to account for the  
256 directional dependency of up- and downwelling shortwave fluxes through the one-layer

257 [atmosphere and found good agreement \(rRMSE < 2% globally\) when benchmarked to online](#)  
258 [radiative transfer calculations. Also considering a directional dependency of the atmospheric](#)  
259 [optical properties, Taylor et al. \(2007\) presented a two-parameter analytical model where](#)  
260 [atmospheric absorption was assumed to occur at a level above atmospheric reflection. The](#)  
261 [analytical model of Donohoe and Battisti \(2011\) subsequently relaxed the directional](#)  
262 [dependency assumption and found the atmospheric attenuation of the surface albedo](#)  
263 [contribution to planetary albedo to be 8% higher than the model of Taylor et al. \(2007\).](#)  
264 [Elsewhere, Qu & Hall \(2006\) developed an analytical framework making use of additional](#)  
265 [atmospheric properties such as cloud cover fraction, cloud optical thickness, and the clear-sky](#)  
266 [planetary albedo, which proved highly accurate when model estimates of planetary albedo](#)  
267 [were evaluated against climate models and satellite-based datasets.](#)

268 [ec. Simple \*kernel-empirical\* parameterizations of the LULCC science community](#)

269 Two [simplified simple empirical](#) parameterizations of shortwave radiative transfer have been  
270 [widely](#) applied within the LULCC science community for estimating  $\Delta F$  from  $\Delta\alpha_s$  (Muñoz  
271 et al., 2010; Lutz et al., 2015; Bozzi et al., 2015; Caiazzo et al., 2014; Cherubini et al.,  
272 2012; Carrer et al., 2018). [While these parameterizations are also based on a single-layer](#)  
273 [atmosphere model of shortwave radiative transfer, At](#) the core of these parameterizations is  
274 the fundamental assumption that radiative transfer is wholly independent of (or unaffected by)  
275  $\Delta\alpha_s$ . In other words, they neglect the change in the attenuating effect of multiple reflections  
276 between the surface and the atmosphere that accompanies a [change to the](#) surface albedo  
277 [change. Nevertheless, due to their simplicity and ease of application they continue to be](#)  
278 [widely employed in climate research. Although not referred to as “kernels” in the literature,](#)  
279 [we present them as such to ensure consistency in notation and terminology henceforth. These](#)  
280 [are subsequently included in the kernel evaluation exercise presented in Section 4.](#)

281

282 The first simplified kernel presented in Muñoz et al. (2010) makes use of a local two-way  
 283 transmittance factor based on the local clearness index (defined in Table 1):

$$284 \frac{\partial SW_{\uparrow}^{TOA}}{\partial \alpha_s} \Delta \alpha_s \equiv K_{\alpha}^{M10} \Delta \alpha_s = SW_{\downarrow}^{TOA} T^2 \Delta \alpha_s \quad (5)$$

285 where  $SW_{\downarrow}^{TOA}$  is the local incoming solar flux at TOA,  $T$  is the local clearness index, and  
 286  $\partial SW_{\uparrow}^{TOA} / \partial \alpha$  is the approximated change in the upwelling shortwave flux at TOA due to a  
 287 change in albedo at the surface.

288

289 The second simplified kernel proposed in Cherubini et al. (2012) makes direct use of the solar  
 290 flux incident at the surface  $SW_{\downarrow}^{SFC}$  combined with a one-way transmission constant  $k$ :

$$291 \frac{\partial SW_{\uparrow}^{TOA}}{\partial \alpha_s} \Delta \alpha_s \equiv K_{\alpha}^{C12} \Delta \alpha_s = SW_{\downarrow}^{SFC} k \Delta \alpha_s \quad (6)$$

292 where  $k$  is based on the global annual mean share of surface reflected shortwave radiation  
 293 exiting a clear sky (Lacis and Hansen, 1974; Lenton and Vaughan, 2009) and is hence  
 294 temporally and spatially invariant. This value – or 0.85 – is similar to the global mean ratio  
 295 of forward to total shortwave scattering reported in Iqbal (1983). Bright & Kvælevåg (2013)  
 296 evaluated Eq. (6) at several locations and found large biases for some regions and months,  
 297 despite good overall performance globally (normalized RMSE = 7%;  $n = 120$  months).

298

299 3. [Methods](#)[Kernel model candidates](#)

300 The six candidate models (or parameterizations) for a CERES-based albedo change kernel  
301 (CACK) are presented henceforth. All requisite variables and their derivatives may be  
302 obtained directly from the CERES EBAF v4 products (at monthly and  $1^\circ \times 1^\circ$  resolution) and  
303 are presented in Table 2. To improve readability, temporal and spatial indexing is neglected  
304 and all terms presented henceforth in Section 3 denote the monthly pixel means.

305 <Table 2>

306 Simple analytical models developed by the climate science community treat the atmosphere  
307 as a single layer having various optical properties. These models vary by the number and type  
308 of optical properties included, whether these have a directional dependency (i.e., isotropic or  
309 anisotropic), or whether inputs other than those derived from the boundary fluxes are required  
310 (i.e., cloud properties). These models are adapted here to derive kernels analytically for  $\Delta\alpha_s$ .

311 a. *CERES isotropic Analytical kernels*

312 The first kernel candidate may be analytically-derived from the CERES EBAF all-sky  
313 boundary fluxes and their derivatives. The surface contribution to the outgoing shortwave  
314 flux at TOA  $SW_{\uparrow,SFC}^{TOA}$  is given can be expressed -(Stephens et al., 2015;Donohoe and Battisti,  
315 2011;Winton, 2005) as:

$$316 \quad SW_{\uparrow,SFC}^{TOA} = SW_{\downarrow}^{TOA} \alpha_s \frac{(1-r-a)^2}{(1-r\alpha_s)} \quad (75)$$

317 where  $r$  is a single pass atmospheric reflection coefficient,  $a$  is a single pass atmospheric  
318 absorption coefficient,  $SW_{\downarrow}^{TOA}$  is the extraterrestrial (downwelling) shortwave flux at TOA,  
319 and  $\alpha_s$  is the surface albedo (defined in Table 42). The expression in the denominator of the  
320 righthand term represents a fraction attenuated by multiple reflections between the surface  
321 and the atmosphere. This model assumes that the atmospheric optical properties  $r$  and  $a$  are

322 insensitive to the origin and direction of shortwave fluxes – or in other words – that they are  
323 isotropic.

324 The single-pass reflectance coefficient is calculated from the system boundary fluxes (Table  
325 [42](#)) following Winton (2005) and Kashimura *et al.* (2017):

$$326 \quad r = \frac{SW_{\downarrow}^{TOA} SW_{\uparrow}^{TOA} - SW_{\downarrow}^{SFC} SW_{\uparrow}^{SFC}}{SW_{\downarrow}^{TOA 2} - SW_{\uparrow}^{SFC 2}}$$

327 [\(86\)](#)

328 while the single-pass absorption coefficient  $a$  is given as:

$$329 \quad a = 1 - r - T(1 - \alpha_s r)$$

330 [\(97\)](#)

331 where  $T$  is the clearness index [defined in](#) [Table 42](#). Our interest is in quantifying  
332 the  $SW_{\uparrow, SFC}^{TOA}$  response to an albedo perturbation at the surface – or the partial derivative of

333  $SW_{\uparrow, SFC}^{TOA}$  with respect to  $\alpha$  in Eq. [\(75\)](#):

$$334 \quad \frac{\partial SW_{\uparrow}^{TOA}}{\partial \alpha_s} \Delta \alpha_s = K_{\alpha_s}^{ISO} \Delta \alpha_s = \frac{SW_{\downarrow}^{TOA} (1 - r - a)^2}{(1 - r \alpha_s)^2} \Delta \alpha_s$$

335 [\(108\)](#)

336 where  $K_{\alpha_s}^{ISO}$  is referred to henceforth as the [CERES \*i\*/isotropic kernel](#).

337  
338 [The second analytical kernel is based on the model of Qu and Hall \(2006\) which makes use of](#)  
339 [auxiliary cloud property information commonly provided in satellite-based products of](#)  
340 [Earth's radiation budget – including CERES EBAF – such as cloud cover area fraction, cloud](#)  
341 [visible optical depth, and clear-sky planetary albedo. This model links all-sky and clear-sky](#)

342 effective atmospheric transmissivities of the earth system through a linear coefficient  $k$   
343 relating the logarithm of cloud visible optical depth to the effective all-sky atmospheric  
344 transmissivity:

$$345 \quad k = \frac{(T_{a,CLR}) - (T_a)}{\ln(\tau + 1)} \quad (9)$$

Field Code Changed

346 where  $T_{a,CLR}$  is the clear-sky effective system transmissivity,  $T_a$  is the all-sky effective system  
347 transmissivity, and  $\tau$  is the cloud visible optical depth. This linear coefficient can then be  
348 used together with the cloud cover area fraction to derive a shortwave kernel based on the  
349 model of Qu and Hall (2006) – or  $K_{\alpha_s}^{QH06}$ :

Field Code Changed

Field Code Changed

Field Code Changed

Field Code Changed

$$350 \quad \frac{\partial SW_{\uparrow}^{TOA}}{\partial \alpha_s} \Delta \alpha_s = K_{\alpha_s}^{QH06} \Delta \alpha_s = SW_{\downarrow}^{SFC} [(T_a) - kc \ln(\tau + 1)] \Delta \alpha_s \quad (10)$$

Field Code Changed

351 where  $c$  is the cloud cover area fraction.

352 b. CERES anisotropic Semi-empirical kernel

353 The second-third kernel makes use of three directionally-dependent (anisotropic) bulk optical  
354 properties  $r_{\uparrow}$ ,  $t_{\uparrow}$ , and  $t_{\downarrow}$ , where the first is the atmospheric reflectivity to upwelling  
355 shortwave radiation and the latter two are the atmospheric transmission coefficients for  
356 upwelling and downwelling shortwave radiation, respectively (Winton, 2005). It is not  
357 possible to derive  $r_{\uparrow}$  analytically from the CERES-all-sky boundary fluxes; however, Winton  
358 (2005) provides an empirical formula relating upwelling reflectivity  $r_{\uparrow}$  to the ratio of all-sky  
359 to clear-sky fluxes incident at surface:

$$360 \quad r_{\uparrow} = 0.05 + 0.85 \left( 1 - \frac{SW_{\downarrow}^{SFC}}{SW_{\downarrow,CLR}^{SFC}} \right) \quad (11)$$

361 where  $SW_{\downarrow, CLR}^{SFC}$  is the clear-sky shortwave flux incident at the surface.

362 Knowing  $r_{\uparrow}$ , we can then solve for the two remaining optical parameters needed to [derive](#)  
363 [obtain](#) our kernel:

$$364 t_{\downarrow} = \frac{SW_{\downarrow}^{SFC} - r_{\uparrow} SW_{\uparrow}^{SFC}}{SW_{\downarrow}^{TOA}}$$

365 [\(4112\)](#)

$$366 t_{\uparrow} = T_a - [t_{\downarrow} - t_{\downarrow}(1 - r_{\uparrow}\alpha_s)]$$

367 [\(4213\)](#)

368 where  $T_a$  is the effective atmospheric transmittance (Table 42) of the earth system.

369 The [anisotropic](#) kernel  $-K_{\alpha_s}^{ANISO}$  [can](#) [may](#) now be [derived](#) [expressed](#) as:

$$370 \frac{\partial SW_{\uparrow}^{TOA}}{\partial \alpha_s} \Delta \alpha_s = K_{\alpha_s}^{ANISO} \Delta \alpha_s = \frac{SW_{\downarrow}^{TOA} t_{\downarrow} t_{\uparrow}}{(1 - r_{\uparrow}\alpha_s)^2} \Delta \alpha_s$$

371 [\(4314\)](#)

372 where  $\underline{K_{\alpha_s}^{ANISO}}$  is henceforth referred to as the *Anisotropic kernel*.

373 c. [CERES a](#)Existing empirical parameterizations[auxiliary input kernel](#)

374 Although not referred to as “kernels” in the literature per se, we present themthe simple  
375 empirical parameterizations as such to ensure consistency inwith previously described  
376 notation and terminology henceforth. These are subsequently included in the kernel  
377 evaluation exercise presented in Section 4.

378

379

380 The first simplified kernel candidate parameterization, originally presented in Muñoz *et al.*  
381 (2010), makes use of a local two-way transmittance factor based on the local clearness index  
382 (defined in Table 1):

$$383 \frac{\partial SW_{\uparrow}^{TOA}}{\partial \alpha_s} \Delta \alpha_s \equiv K_{\alpha_s}^{M10} \Delta \alpha_s = SW_{\downarrow}^{TOA} T^2 \Delta \alpha_s$$

384 (15)

385 where  $SW_{\downarrow}^{TOA}$  is the local incoming solar flux at TOA,  $T$  is the local clearness index, and  
386  $\partial SW_{\uparrow}^{TOA} / \partial \alpha_s$  is the approximated change in the upwelling shortwave flux at TOA due to a  
387 change in albedo at the surface albedo.

388

389 The second simplified kernel candidate parameterization, originally proposed in Cherubini *et*  
390 *al.* (2012), makes direct use of the solar flux incident at the surface  $SW_{\downarrow}^{SFC}$  combined with a  
391 one-way transmission constant  $k$ :

$$392 \frac{\partial SW_{\uparrow}^{TOA}}{\partial \alpha_s} \Delta \alpha_s \equiv K_{\alpha_s}^{C12} \Delta \alpha_s = SW_{\downarrow}^{SFC} k \Delta \alpha_s \quad (16)$$

393 where  $k$  is based on the global annual mean share of surface reflected shortwave radiation  
394 exiting a clear-sky (Lacis and Hansen, 1974; Lenton and Vaughan, 2009) and is hence  
395 temporally and spatially invariant. This value – or 0.85 -- is similar to the global mean ratio  
396 of forward-to-total shortwave scattering reported in Iqbal (1983). Bright & Kvalevåg (2013)  
397 evaluated Eq. (16) at several global locations and found large biases for some regions and  
398 months, despite good overall performance globally (normalized RMSE = 7%;  $n = 120$   
399 months).

400

401 Qu and Hall (2006) developed an alternative analytical kernel to the two described above.  
402 The model makes use of auxiliary cloud property information commonly provided in satellite-  
403 based products of Earth's radiation budget including CERES EBAF such as cloud cover  
404 area fraction, cloud visible optical depth, and clear sky planetary albedo. The model links all-  
405 sky and clear sky effective atmospheric transmissivities of the earth system through a linear  
406 coefficient  $k$  relating the logarithm of cloud visible optical depth to the effective all-sky  
407 atmospheric transmissivity:

408 
$$(14)$$

409 where  $T_{a,CLR}$  is the clear sky effective system transmissivity,  $T_a$  is the all-sky effective system  
410 transmissivity, and  $\tau$  is the cloud visible optical depth. This linear coefficient can then be  
411 used together with the cloud cover area fraction to derive a shortwave kernel based on the  
412 model of Qu and Hall (2006) or  $K_{\alpha_s}^{QH06}$ :

413 
$$(15)$$

414 where  $c$  is the cloud cover area fraction.

415

416 d. CERES statistical kernelNovel empirical parameterization

417 To determine whether the GCM-based kernels could be approximated with sufficient fidelity  
418 using even other simpler model formulations based on the CEREStheir own boundary data,  
419 we applied machine learning to identify potential model forms using GCM boundary fluxes as  
420 input. For the two GCMs kernels in which the GCM's own boundary fluxes are also made  
421 available (CAM5 and ECHAM6), we used machine learning to the CERES EBAF all-sky  
422 boundary fluxes (or system parameters derived from these fluxes) that minimized the sum of  
423 squared residuals between monthly meanthe four shortwave boundary fluxes and the GCM  
424 kernel at the monthly time stepof four GCM-based kernels (described below) and model

425 estimates. The reference dataset consisted of a random global sample of 50200,000 (~50%)  
426 2.8° x 2.8° grid cells at native model resolution (97% and 32% of all cells for ECHAM6 and  
427 CAM5, respectively), from the multi-GMC mean, of which 50% were used for training and  
428 50% for validation. Models were identified using a form of genetic programming known as  
429 symbolic regression (Eureqa®; Nutonian Inc.; (Schmidt and Lipson, 2009, 2010)) which  
430 searches a wide space of for both optimal model structures as constrained by user input and  
431 efficiencies. In our case, we allowed the model to include the operators (i.e., addition,  
432 subtraction, multiplication, division, sine, cosine, tangent, exponential, natural logarithm,  
433 factorial, power, square root), but numerical coefficients were forbidden. The model search  
434 was allowed to continue until the percent convergence and maturity metrics exceeded 98%  
435 and 50%, respectively, at which point more than  $1 \times 10^{11}$  formulae had been evaluated. A  
436 parsimonious solution was chosen by minimizing the error metric and model complexity  
437 using the Pareto front (Figure S1 of Supporting Information) (Smits and Kotanchek, 2005).

438 Between CAM5 and ECHAM6, four common model solutions were found (Table S1 of  
439 Supporting Information). The best of these common solutions is subsequently referred to as

440  $K_{\alpha_s}^{BO18}$  and is given as Based on the mean squared deviation (MSD) and Akaike's information

Field Code Changed

441 criterion (AIC), the best model form of the statistical kernel — subsequently referred to as

442  $K_{\alpha_s}^{BO18}$  — is given as:

$$443 \frac{\partial SW_{\uparrow}^{TOA}}{\partial \alpha_s} \Delta \alpha_s = K_{\alpha_s}^{BO18} \Delta \alpha_s = SW_{\downarrow}^{SFC} \sqrt{T} \Delta \alpha_s$$

444 (4617)

445

446

447 subsequently referred to as  $K_{\alpha_s}^{BO18}$  — is given as 4. Kernel model evaluation

448 *d. Initial screening of candidate models for a CERES based kernel*

449 Four GCM kernels are employed as benchmarks to initially screen the six CERES based  
450 kernel model candidates: the Community Atmosphere Model version 3, or CAM3 (Shell et  
451 al., 2008), the Community Atmosphere Model version 5, or CAM5 (Pendergrass et al., 2018),  
452 the European Center and Hamburg model version 6, or ECHAM6 (Bleck and Mauritzen,  
453 2014), and the Geophysical Fluid Dynamics Laboratory model version AM2p12b, or GFDL  
454 (Soden et al., 2008). The four GCM kernels vary in vertical and horizontal resolution,  
455 parameterization of shortwave radiative transfer, and year of atmospheric state (input  
456 variables).

457

458 *a. Initial candidate screening*

459 The four GCM kernels presented in Section 2.b are employed as benchmarks to initially  
460 screen the six simple model candidates. We compute a skill metric analogous to the “relative  
461 error” metric used to evaluate GCMs by Anav et al. (2013) that takes into account error in the  
462 spatial pattern between a model and an observation. Because we have no true observational  
463 reference, our evaluation instead focuses on the disagreement or deviation between CERES  
464 and GCM kernels at the monthly time step. Given interannual climate variability in the earth  
465 system, the challenge of comparing the multi-year CERES kernel to a single-year GCM  
466 kernel can be partially overcome by averaging the four GCM kernels.

467

468 Using the multi-GCM mean as the reference, we first compute the absolute deviation  $AD_{m,p}^X$

469 as:

470  $AD_{m,p}^X = |CERES_{m,p}^X - \overline{GCM}_{m,p}|$

471 (4718)

472 where  $CERES_{m,p}^X$  is the kernel for CERES model candidate X-x in month  $m$  and pixel  $p$  and

473  $\overline{GCM}_{m,p}$  is the multi-GCM mean of the same pixel and month.  $AD_{m,p}^X$  is then normalized to

474 the maximum absolute deviation of all six CERES kernels for the same pixel and month to

475 obtain a normalized absolute deviation,  $NAD_{m,p}^X$ , which is analogous to the “relative error”

476 metric of Anav et al. (2013) with having values ranging between 0 and 1:

477  $NAD_{m,p}^X = 1 - \frac{AD_{m,p}^X}{\max(AD_{m,p})}$

478 (4819)

479 where  $\max(AD_{m,p})$  is the maximum absolute deviation of all six CERES kernels at pixel  $p$

480 and month  $m$ .

481

482 CERES kernel ranking is based on the mean relative absolute deviation in both space and time

483 – or  $\overline{NAD}^X$ :

484  $\overline{NAD}^X = \frac{1}{M} \sum_{m=1}^M \frac{1}{P} \sum_{p=1}^P NAD_{m,p}^X$

485 (4920)

486 where  $M$  is the total number of months (i.e., 12) and  $P$  is the total number of grid cells.

487

488 eb. GCM kernel emulation

489 In order to eliminate any bias related to differences in the atmospheric state embedded in the  
490 GCM and CERES derived kernels input climatologies, we re-compute our simple  
491 kernels emulate them by applying the candidate models (or parameterizations) using the  
492 original GCM boundary fluxes as input. Emulation is only done for two of GCM-based  
493 kernels since only two of them have provided the accompanying same shortwave boundary  
494 fluxes used to compute the two most recent albedo change kernels based boundary fluxes  
495 needed to do so: – on ECHAM6 (Block and Mauritsen, 2014) and CAM5 (Pendergrass et al.,  
496 2018). This Emulation enables a more critical evaluation of the functional form of the  
497 candidates simple models in relation to the more sophisticated radiative transfer schemes  
498 employed by ECHAM6 (Stevens et al., 2013) and CAM5 (Hurrell et al., 2013).

499 c. CACK model uncertainty

500 Following emulation, monthly GCM kernels are then regressed on the monthly kernels  
501 emulated with the leading model candidates. The model that best emulates both GCM kernels  
502 – as measured in terms of the mean coefficient of determination ( $R^2$ ) and mean RMSE – is  
503 chosen to represent CACK.

504 Three sources of uncertainty are considered for CACK when based on the CERES boundary  
505 flux climatology (i.e., 2001-2016 monthly means): 1) physical variability 2) data uncertainty;  
506 and 3) model error (Mahadevan and Sarkar, 2009) The first is related to the interannual  
507 variability of Earth's atmospheric state and boundary radiative fluxes. The second is related  
508 to the uncertainty of the CERES EBAF v4 variables used as input to CACK (including  
509 measurement error). The third source of uncertainty is the error related to CACK's model  
510 form. CACK's combined uncertainty for any given pixel and month is estimated as follows,  
511 where if CACK or  $y$  is some non-linear function of the CERES boundary inputs  $x_1$  and  $x_2$   
512 that co-vary in time and space, then the combined uncertainty of  $y$  – or  $\sigma(y)$  – may be

Field Code Changed  
Field Code Changed

513 expressed as the sum of the *model error* plus the combined *physical variability* and *data*  
514 *uncertainty* associated with  $x_1$  and  $x_2$  summed in quadrature (Clifford, 1973; Breipohl,  
515 1970; Green et al., 2017):

$$516 \sigma(y) \approx \sigma_{ME}(y) + \sqrt{\left(\frac{\partial y}{\partial x_1}\right)^2 [\sigma_{PV}(x_1) + \sigma_{DU}(x_1)]^2 + \left(\frac{\partial y}{\partial x_2}\right)^2 [\sigma_{PV}(x_2) + \sigma_{DU}(x_2)]^2 + \sqrt{\left(2 \frac{\partial y}{\partial x_1} \frac{\partial y}{\partial x_2} \sigma(x_1, x_2)\right)^2}} \quad (21)$$

517 where  $\sigma_{PV}(x_1)$  and  $\sigma_{PV}(x_2)$  are the standard deviations of the 16-yr. climatological record of  
518 CERES input variables  $x_1$  and  $x_2$ , respectively, for a given grid cell and month,  $\sigma_{DU}(x_1)$  and  
519  $\sigma_{DU}(x_2)$  are the absolute uncertainties of CERES input variables  $x_1$  and  $x_2$ , respectively, for  
520 a given grid cell and month,  $\sigma(x_1, x_2)$  is the covariance within the 16-yr. climatological  
521 record between CERES input variables  $x_1$  and  $x_2$  for a given month and grid cell, and  $\sigma_{ME}$  is  
522 the monthly grid cell model error. Model error ( $\sigma_{ME}(y)$ ) and data uncertainties ( $\sigma_{DU}(x_n)$ )  
523 for any given grid cell and month are based on the relative RMSE (Supporting Information)  
524 and relative uncertainties of CERES boundary terms reported in Kato et al. (2018) (cf. Table  
525 8, “Monthly gridded, Ocean + Land”) and Loeb et al. (2017) (cf. Table 8, “All-sky, Terra-  
526 Aqua period”). For the model error, we take the mean relative RMSE of the machine learning  
527 model solutions for ECHAM5 and CAM5. For the relative uncertainty of the incoming solar  
528 flux at TOA ( $SW_{\downarrow}^{TOA}$ ), we use the 1% “calibration uncertainty” reported in Loeb et al. (2017).

529 If CACK’s intended application is to estimate a temporally-explicit  $\Delta F$  within the CERES era  
530 (i.e., if temporally-explicit rather than the climatological mean CERES boundary fluxes are  
531 desired to compute CACK), the uncertainty related to *physical variability* ( $\sigma_{PV}(x_n)$ ) can be  
532 dropped from Eq. (21).

Field Code Changed  
Field Code Changed

Field Code Changed

Field Code Changed  
Field Code Changed

Field Code Changed

Field Code Changed

Field Code Changed

Field Code Changed

Field Code Changed

Field Code Changed

Field Code Changed

Field Code Changed

Field Code Changed

Field Code Changed

Field Code Changed

Field Code Changed

Field Code Changed

Field Code Changed

Field Code Changed

533 *d. Climatological CACK example application*

534 To demonstrate CACK's application when based on monthly CERES EBAF climatology,  
535 including the handling of uncertainty, we estimate the annual mean  $\Delta F$  from a  $\Delta\alpha$  scenario

Field Code Changed

536 associated with hypothetical deforestation in the tropics, where  $\Delta F$  for a given month is

537 estimated as Eq. (4) where  $K_{\alpha_s}$  is the 2001-2016 monthly climatological CACK and  $\Delta\alpha$  is

Field Code Changed

Field Code Changed

538 the difference in the 2001-2011 monthly climatological mean white-sky surface albedo  
539 between "Croplands" (CRO) and "Evergreen broadleaved forests" (EBF) taken from Gao *et*  
540 *al.* (2014) which is based on International Geosphere-Biosphere Program definitions of land  
541 cover classification.

542 The monthly climatological albedo look-up maps of Gao *et al.* (2014) contain their own  
543 uncertainties, which we take as the mean absolute difference between the monthly albedos  
544 reconstructed using their look-up model and the monthly MODIS retrieval record (c.f. Table 3  
545 in Gao *et al.* (2014)).

546 The total estimated uncertainty linked to the annual local (i.e., grid cell) instantaneous  $\Delta F$  can  
547 thus be expressed (in  $\text{W m}^{-2}$ ) as:

$$548 \sigma(\Delta F) = \frac{1}{12} \sum_{m=1}^{12} |\Delta F_m| \sqrt{\left( \frac{\sigma(K_{\alpha_s, m})}{K_{\alpha_s, m}} \right)^2 + \left( \frac{\sigma(\Delta\alpha_{s, m})}{\Delta\alpha_{s, m}} \right)^2} \quad (22)$$

Field Code Changed

549 where  $\sigma(K_{\alpha_s, m})/K_{\alpha_s, m}$  is the relative grid cell uncertainty of CACK and  $\sigma(\Delta\alpha_{s, m})/\Delta\alpha_{s, m}$  is  
550 the relative uncertainty of  $\Delta\alpha_s$  in month  $m$  defined as:

Field Code Changed

Field Code Changed

Field Code Changed

$$551 \frac{\sigma(\Delta\alpha_{s, m})}{\Delta\alpha_{s, m}} = \sqrt{\left( \frac{\sigma(\alpha_{s, m})}{\alpha_{CRO, m}} \right)^2 + \left( \frac{\sigma(\alpha_{s, m})}{\alpha_{EBF, m}} \right)^2} \quad (23)$$

Field Code Changed

552 where  $\sigma(\alpha_{s,m})$  is the monthly absolute uncertainty of the climatological mean surface albedo  
553 (i.e., of the Gao *et al.* (2014) product).

Field Code Changed

554 *e. Temporally-explicit CACK application example*

555 Use of a temporally-explicit CACK may be desirable for time-sensitive applications within  
556 the CERES era. This is particularly true for regions experiencing significant changes to the  
557 atmospheric state affecting shortwave radiation transfer. A good example is in southern  
558 Amazonia where tropical deforestation has been linked to changes in cloud cover (Durieux et  
559 al., 2003; Lawrence and Vandecar, 2014; Wright et al., 2017). To exemplify this, we estimate  
560 the annual mean instantaneous  $\Delta F$  for CERES grid cells in the region having experienced  
561 significant trends in both surface albedo and cloud area fraction during the 2001-2016 period.  
562 Grid cell trends in surface albedo and cloud area fraction are deemed significant if the slopes  
563 of linear fits obtained from local (i.e., grid cell) ordinary least squares regressions had p-  
564 values  $< 0.05$ . We then apply the slope of the surface albedo trend to represent the monthly  
565 mean interannual  $\Delta\alpha$  incurred over the time series together with CACK updated monthly to  
566 estimate the local annual mean instantaneous  $\Delta F$  at each step in the series:

$$567 \Delta F(t) = \sum_{m=1}^{m=12} -K_{\alpha_s,m}(t) \Delta\alpha_s \quad (24)$$

568 where  $K_{\alpha_s,m}(t)$  is the monthly CACK in year  $t$  of the time series.  $\Delta F$  is then averaged across

Field Code Changed

569 all grid cells in the sample, with the results then compared to the  $\Delta F$  that is computed for the

570 same grid sample using the time-insensitive CAM5 and ECHAM6 kernels (i.e.,  $K_{\alpha_s,m} \neq f(t)$ ).

Field Code Changed

571 Using the slope of the surface albedo trend as the  $\Delta\alpha_s$  for all months and years rather than the

Field Code Changed

572 actual  $\Delta\alpha_{s,m}(t)$  (i.e.,  $\Delta\alpha_{s,m}(t) = \alpha_{s,m,t} - \alpha_{s,m,t-1}$ ) yields the same result when averaged over the

Field Code Changed

573 full time period but allows us to isolate the effect of the changing atmospheric state on

Field Code Changed

574 calculations of  $\Delta F$ . We limit the  $\Delta F$  uncertainty estimate to CACK's uncertainty that includes

575  $\sigma_{DU}(x_n)$  and  $\sigma_{ME}(x_n)$  but excludes  $\sigma_{PV}(x_n)$

Field Code Changed  
Field Code Changed  
Field Code Changed

576 **45. Results**

577

578 *a. Initial performance screening*

579 *a. Initial kernel performance screening*

580 Seasonally, differences in latitude band means between the CERES the CERES kernel

581 candidates and the multi-GCM mean kernels are shown in Figure 1.

582

583 <Figure 1>

584

585 Qualitatively, starting with December-January-February (DJF),  $K_{\alpha_s}^{BO18}$  gives the best

586 agreement with  $K_{\alpha_s}^{\overline{GCM}}$  with the exception of the zone around  $55 - 65^{\circ}\text{S}$  ( $-55 - -65^{\circ}$ ), where

587  $K_{\alpha_s}^{QH06}$  gives slightly better agreement (Fig. 1A). In March-April-May (MAM),  $K_{\alpha_s}^{BO18}$  appears

588 to give the best overall agreement with the exception of the high Arctic, where  $K_{\alpha_s}^{ANISO}$  and

589  $K_{\alpha_s}^{C12}$  give better agreement, and with the exception of the zone around  $60 - 65^{\circ}\text{S}$  ( $-60 - -65^{\circ}$ )

590 where  $K_{\alpha_s}^{QH06}$ ,  $K_{\alpha_s}^{ANISO}$ , and  $K_{\alpha_s}^{C12}$  agree best with  $K_{\alpha_s}^{\overline{GCM}}$  (Fig. 1B). The largest spread in

591 disagreement across all six CERES kernels is found in June-July-August (JJA; Fig. 1 C) at

592 northern high latitudes.  $K_{\alpha_s}^{BO18}$  appears to agree best both here and elsewhere with the

593 exception of the zone between  $\sim 20 - 35^{\circ}\text{N}$ , where  $K_{\alpha_s}^{QH06}$  gives slightly better agreement.

594 In September-October-November (SON),  $K_{\alpha_s}^{BO18}$  agrees best with  $K_{\alpha_s}^{\overline{GCM}}$  at all latitudes except

595 the zone between  $10 - 25^{\circ}\text{N}$  and  $55 - 65^{\circ}\text{S}$  where  $K_{\alpha_s}^{QH06}$  agrees slightly better.

596

597 Quantitatively, the proportion of the total variance explained by linear regressions of monthly  
598  $K_{\alpha_s}^{\overline{GCM}}$  on monthly  $K_{\alpha_s}^{CERES}$  (i.e.,  $\overline{R^2}$ ) is highest and equal for the CERES kernels based on the  
599 ANISO, QH06, and BO18 models (Fig. 2 B, C, & D). Of these three,  $K_{\alpha_s}^{QH06}$  has a y-intercept  
600 ( $\overline{B_0}$ ) closest to 0 and a slope ( $\overline{m}$ ) of 1, although the root mean squared deviation-error  
601 (RMSDRMSE) – an accuracy measure – is slightly better (lower) for  $K_{\alpha_s}^{BO18}$ . The two  
602 CERES kernels with the lowest  $R^2$ , highest slopes (negative deviations), highest  
603 RMSDRMSE, and y-intercepts with the largest absolute difference from zero – or the worst  
604 performing candidates – are those based on the ISO and M10 models (Fig. 2 A&E).

605

606 < Figure 2 >

607  
608 Although the y-intercept deviation from 0 for  $K_{\alpha_s}^{C12}$  is relatively low, its RMSD is ~50%  
609 higher than that of  $K_{\alpha_s}^{QH06}$ ,  $K_{\alpha_s}^{BO18}$ , and  $K_{\alpha_s}^{ANISO}$  and leads to notable positive deviation from the  
610 multi-GCM mean ( $K_{\alpha_s}^{\overline{GCM}}$ ) judging by its slope of 0.92.

611

612 e. Normalized absolute deviation

613 Globally, NAD for the QH06, ANISO, and BO18 kernels are far superior to the ISO, M10,  
614 and C12 kernels (Table 23).

615

616 < Table 23 >

617  
618 After filtering to remove grid cells for oceans and other water bodies, NAD scores for these  
619 three kernels decreased; the decrease was smallest for  $K_{\alpha_s}^{BO18}$  (-0.03) and largest for  $K_{\alpha_s}^{QH06}$  (-

620 0.06). Despite constraining the analysis to land surfaces only, the rank order remained

621 unchanged (Table 23), and  $K_{\alpha_s}^{QH06}$ ,  $K_{\alpha_s}^{BO18}$ , and  $K_{\alpha_s}^{ANISO}$  are subjected to further evaluation.

622

Field Code Changed  
Field Code Changed  
Field Code Changed

623 *db. GCM kernel emulation and additional performance screening evaluation*

624 However, Because the simple kernel based on the QH06 model ( $K_{\alpha_s}^{QH06}$ ) required auxiliary

625 inputs for cloud cover area fraction and cloud optical depth – two atmospheric state variables

626 not provided with the ECHAM6 and CAM5 kernel datasets – it was not possible to emulate

627 these two GCM kernels using with  $K_{\alpha_s}^{QH06}$  the QH06 model. Additional performance

628 evaluation through GCM kernel emulation is therefore restricted to the ANISO and BO18

629 models.

630 < Figure 3 >

631 Globally, the kernel based on the ANISO model displays larger annual mean biases relative to

632 BO18 when compared to both ECHAM6 and CAM5 kernels (Figure 3). Notable positive

633 biases over land with respect to both ECHAM6 and CAM5 kernels are evident in the northern

634 Andes region of South America, the Tibetan plateau, and the tropical island region comprising

635 Indonesia, Malaysia, and Papua New Guinea (Fig. 3 A & C). Notable negative biases over

636 land with respect to both ECHAM6 and CAM5 kernels are evident over Greenland,

637 Antarctica, northeastern Africa, and the Arabian Peninsula (Fig. 3 A & C).

638 < Figure 4 >

639 Globally, annual biases for BO18 are generally found to be lower than for ANISO and are

640 mostly non-existent in extra-tropical ocean regions (Fig. 3 B & D). Patterns in biases over

641 land are mostly negative with the exception of Saharan Africa where the annual mean bias

642 with respect to both GCMs is positive. For BO18, systematic positive biases – or biases  
643 evident with respect to both GCM kernels – appear over eastern tropical and subtropical  
644 marine coastal upwelling zones where marine stratocumulus cloud dynamics are difficult for  
645 GCMs to resolve (Bretherton et al., 2004; Richter, 2015).

646 < Table 34 >

647 ~~Performance metrics based on regressing monthly kernels from the two GCMs on kernels~~  
648 ~~emulated with both ANISO and BO18 models~~~~Regression statistics (Figure 4)~~ indicate a  
649 greater overall ~~accuracy (or agreement)~~~~performance~~ for BO18 (Figure 4) than for ANISO.  
650 ~~RMSDs–RMSEs~~ for monthly kernels emulated with BO18 are 9.0 and 8.2 W m<sup>-2</sup> ~~with respect~~  
651 ~~to~~ for CAM5 and ECHAM6, respectively – which is ~50-60% of the ~~RMSDs–RMSEs~~  
652 emulated with the ANISO model. ~~Relative to ANISO, the BO18 model also gives a higher~~  
653 ~~R<sup>2</sup>, a slope closer to 1, and a y-intercept closer to zero (Figure 4).~~ The BO18 model (or  
654 ~~parameterization~~) is therefore selected for the CERES albedo change kernel (CACK).

655 Focusing ~~henceforth only on the only on the kernel emulated with BO18 model~~~~GCM kernels~~  
656 ~~emulated with~~  $K_{\alpha_s}^{BO18}$  ~~henceforth~~, negative biases are evident in all months (Table 34), with

Field Code Changed

657 the largest biases (in magnitude) appearing in May (-4.4 W m<sup>-2</sup>) and November (-2.5 W m<sup>-2</sup>)  
658 for CAM5 and ECHAM6, respectively. In absolute terms, largest biases of 8.6 W m<sup>-2</sup> and 6.8  
659 W m<sup>-2</sup> appear in June for CAM5 and ECHAM6, respectively. Annually, the mean absolute  
660 bias for CAM5 and ECHAM6 is 6.8 and 6.1 W m<sup>-2</sup>, respectively – a magnitude which seems  
661 remarkably low if one compares this to the annual mean disagreement (standard deviation) of  
662 33 W m<sup>-2</sup> across all four GCM kernels (not shown; ~~for seasonal mean standard deviations see~~  
663 [Fig. 1](#)).

664 [c. CACK uncertainty](#)

665 For a kernel based on 2001-2016 monthly mean CERES EBAF climatology, Figure 5  
666 illustrates the contribution of the absolute error related to  $K_{\alpha_s}^{BO18}$ 's model form (Fig. 5 A,  
667 annual mean) relative to CACK's total absolute uncertainty (Fig. 5 C, annual mean), which  
668 includes the uncertainty surrounding CERES EBAF v4 input variables  $SW_{\downarrow}^{SFC}$  and  $SW_{\downarrow}^{TOA}$   
669 and their interannual variability (Fig. 5 B, annual mean).

Field Code Changed  
Field Code Changed

670 <Figure 5>  
671 Total propagated  $\sigma_{pv}$  and  $\sigma_{du}$  far exceeds  $\sigma_{me}$ , is dominated by  $\sigma_{du}(SW_{\downarrow}^{SFC})$  and  
672  $\sigma_{pv}(SW_{\downarrow}^{SFC})$ , and is largest in the Pacific region to the south of the intertropical convergence  
673 zone (ITCZ). Over land, the annual  $\sigma_{pv}$  and  $\sigma_{du}$  as well as the annual  $\sigma_{total}$  are generally  
674 largest in arid or high altitude regions (Fig. 5 B). However, annual CACK values are also  
675 large in these regions reducing the relative uncertainty (Fig. 5 D). The largest relative  
676 uncertainties over land (on an annual basis) – which can approach 50% – are found over  
677 central Europe, northwestern Asia, southeastern China, Andean Chile, and northwestern N.  
678 America (Fig. 5 D).

Field Code Changed  
Field Code Changed

#### 679 *d. Climatological CACK application*

680 When estimated with a CACK based on monthly CERES EBAF climatology, the annual  $\Delta F$   
681 from  $\Delta\alpha_s$  linked to hypothetical deforestation in the tropics is negative in most regions,  
682 approaching  $-20 \text{ W m}^{-2}$  locally in some regions of the Brazilian Cerrado and south of the  
683 Sahel region in Africa (Fig. 6 B). The combined CACK and  $\Delta\alpha_s$  uncertainty for these  
684 regions can approach  $\pm 5 \text{ W m}^{-2}$  annually (Fig. 6 C) in regions like the Brazilian Cerrado and  
685 sub-Saharan Africa. Relative to the  $\Delta F$  magnitude, however, the largest uncertainties (annual)

Field Code Changed  
Field Code Changed

686 may be found in the subtropical regions of Central America, southern Brazil, southern Asia,  
687 and northern Australia, where it can approach 30-40% (Fig. 6 D).

688 *e. Temporally-explicit CACK application*

689 The effect of a decreasing cloud cover trend in southern Amazonia (Fig. 7 B) on shortwave  
690 radiative transfer and thus a CACK-based estimate of regional mean annual  $\Delta F$  emerges in  
691 Figure 7 C, where  $\Delta F$  increases in magnitude by  $0.004 \text{ W m}^{-2}$  from 2002 to 2016. This  $\Delta F$   
692 trend would otherwise go undetected if a GCM-based kernel were applied to the same surface  
693 albedo trend – that is, to a sustained positive interannual monthly albedo change “pulse”.

694 Alternatively, a CACK based on 2001 CERES EBAF inputs (applied with  $\Delta\alpha_s$  for 2001-

Field Code Changed

695 2002) would give slightly higher  $\Delta F$  estimates relative to those based on ECHAM6 and

696 CAM5 kernels; conversely, a CACK based on 2015 CERES EBAF inputs (applied with  $\Delta\alpha_s$

Field Code Changed

697 for 2015-2016) that would yield lower  $\Delta F$  estimates relative to those based on the same two  
698 GCM-based kernels (Fig. 7 C). Use of temporally-explicit CACK can therefore capture  $\Delta F$   
699 trends related to a changing atmospheric state that fixed-state GCM kernels are unable to  
700 capture.

701 **5. Discussion and conclusions**

702 Motivated by an increasing abundance of climate impact research focusing on land processes  
703 in recent years, we comprehensively evaluated six simplified models (or parameterizations) as  
704 candidates for an albedo change kernel based on the CERES EBAF v4 products (Loeb et al.,  
705 2017; Kato et al., 2018). ~~linking shortwave radiative flux perturbations at TOA with surface~~  
706 ~~albedo changes at the surface~~. Relative to albedo change kernels based on sophisticated  
707 radiative transfer schemes embedded in GCMs, ~~the simplified models evaluated here~~  
708 CERES-based albedo change kernel – or CACK – represents a more transparent and  
709 empirically-rooted alternative that can be updated frequently at relatively low cost ~~using~~

710 boundary fluxes obtained from remote sensing based products of Earth's shortwave energy  
711 budget. This allows greater flexibility to meet the needs of research that focuses on  
712 longer term surface albedo trends within the CERES era in regions currently undergoing  
713 rapid changes in atmospheric composition state as it affects shortwave radiation transfer.  
714 Although some modeling groups have provided recent updates to radiative their albedo  
715 change kernels using the latest GCM versions (e.g., (Pendergrass et al., 2018)), the  
716 atmospheric state of the boundary conditions used to derive them may still be considered  
717 outdated or not in sync with that required for some many applications (Table 1).

718

719 Based on both qualitative and quantitative benchmarking against the mean of four GCM  
720 kernels, the simple novel kernel model parameterization derived obtained from machine  
721 learning,  $K_{\alpha_s}^{BO18}$  BO18, together with the two (semi-)analytically derived models kernels,  
722  $K_{\alpha_s}^{QH06}$  QH06 and  $K_{\alpha_s}^{ANISO}$  ANISO, proved far superior to the  $K_{\alpha_s}^{ISO}$  analytical kernel and to the  
723 two additional empirical parameterizations  $K_{\alpha_s}^{C12}$  and  $K_{\alpha_s}^{M10}$  M10, C12, and the ISO kernel  
724 models. When subjected to additional performance evaluation, however, we found that  $K_{\alpha_s}^{BO18}$

Field Code Changed

725 the BO18 model was able to more robustly emulate the two GCM kernels (ECHAM6 and  
726 CAM5) kernels with exceptionally high accuracy agreement, suggesting that  $K_{\alpha_s}^{BO18}$  this model  
727 could serve as a suitable candidate for an albedo change kernel based on CERES boundary  
728 fluxes CACK.

Field Code Changed

729 Relative to the monthly CAM5 and ECHAM6 kernels, the RMSD mean absolute monthly  
730 emulation "error" of this kernel henceforth referred to as the CERES Albedo Change Kernel  
731 (CACK v1.0) of  $K_{\alpha_s}^{BO18}$  was found to be 6.8 and 6.1 W m<sup>-2</sup> when benchmarked to the

Field Code Changed

732 ~~CAM5 and ECHAM6 kernel~~, respectively – a magnitude which is only ~20% of the standard  
733 deviation found across four GCM kernels [\(annual mean\)](#) [\(annual mean\)](#). CACK's remarkable  
734 simplicity lends support to the idea of using machine learning to explore and detect emergent  
735 properties of ~~shortwave~~ radiative transfer [or other complex, interactive model outputs](#) in  
736 future research. The fact that the  $K_{\alpha_s}^{BO18}$  parameterization emerged as the best common  
737 solution from two independently executed machine learning analyses each employing a  
738 random sampling unique to a specific GCM kernel suggests that the  $K_{\alpha_s}^{BO18}$  parameterization  
739 is robust and insensitive to the underlying GCM representation of shortwave radiative  
740 transfer.

Field Code Changed

741  
742 Despite the stronger empirical foundation of CACK ~~its stronger empirical foundation~~ over a  
743 GCM-based kernel, it is important to recognize CACK's ~~s~~ limitations. Firstly, while CACK  
744 has a finer spatial resolution than most GCM kernels, it still represents a spatially averaged  
745 response rather than a truly local response; in other words, the state variables used to define  
746 the  $SW_{\uparrow}^{TOA}$  response are averages tied to the coarse spatial (i.e.,  $1^{\circ} \times 1^{\circ}$ ) resolution of the  
747 CERES EBAF v4 product grids. Secondly, the monthly CERES EBAF-Surface product used  
748 to define lower atmospheric boundary conditions is not strictly an observation. The space-  
749 borne ~~observation~~ platform is not able to directly ~~observe Earth's surface fluxes~~ observe  
750 surface irradiances, requiring under overcast conditions and hence requires model  
751 augmentation additional satellite-based estimates of cloud and aerosol properties as input to a  
752 radiative transfer model (Kato et al., 2012). However, Although TOA irradiances are applied  
753 to constrain the surface irradiances, the energy balancing step ensures that fluxes are adjusted  
754 to match the observed rate of heat accumulation in the climate system (i.e., the oceans)  
755 (Hansen et al., 2005) they remain susceptible to errors in the radiative transfer model inputs.

Field Code Changed

756 Considering this error as “data uncertainty” increases CACK’s overall uncertainty beyond that  
757 which is related to its underlying parameterization or “model error”. These processes The  
758 uncertainty of CERES surface shortwave irradiances – as well as extensive ground validation  
759 and testing – are documented in greater detail elsewhere (Kato et al., 2013; Loeb et al.,  
760 2009; Loeb et al., 2017; Kato et al., 2018) and may continue to be reduced in future EBAF-  
761 Surface version-s. Further, while CACK has a finer spatial resolution than most GCM  
762 kernels, it still represents a spatially averaged response rather than a truly local response; in  
763 other words, the state variables used to define the response are tied to the coarse spatial (i.e.,  
764  $1^\circ \times 1^\circ$ ) resolution of the CERES EBAF product grids. Lastly, it is important to emphasize  
765 that CACK is based on the climate conditions of the present day (2001–2016); hence, caution  
766 should be exercised when applying it to estimate associated with albedo changes occurring  
767 outside this range.

768 *a. Concluding remarks*

769

770 To conclude, we developed, evaluated, and proposed a radiative kernel for surface albedo  
771 change based on CERES EBAF v4 products – or CACK. Relative to existing kernels based on  
772 GCMs, evaluated six simplified albedo change kernels based on CERES shortwave boundary  
773 fluxes as candidate alternatives to GCM-based albedo change kernels. Albedo change  
774 kernels are useful tools for estimating instantaneous shortwave radiative forcings connected to  
775 anthropogenic land use activities. Our results showed that the BO18 model developed and  
776 presented in this study is the best candidate for a CERES albedo change kernel – or CACK.  
777 CACK provides a higher spatial resolution, higher transparency alternative to existing kernels  
778 based on GCMs that is more amenable to user needs. For LULCC research of the near-past,  
779 present day, or near-future periods, application of a CACK whose inputs are based on

780 monthly climatological means of the full CERES EBAF record can better-account for the  
781 corresponding interannual variability in Earth's atmospheric state affecting shortwave  
782 radiative transfer. For regions undergoing changes in atmospheric state that are detectable  
783 above the normal variability within the CERES era, application of a temporally-explicit  
784 CACK can better-account for its influence on  $\Delta F$  estimates from surface albedo change.  
785 CACK's input flexibility and transparency combined with documented uncertainty make it  
786 well-suited to be applied~~CACK could be easily applied~~ as part of a Monitoring, Reporting,  
787 and Verification (MRV) frameworks for biogeophysical impacts on land, analogous to those  
788 which currently exist for land sector greenhouse gas emissions.

789 ~~Given the extensive time span of the CERES EBAF products, CACK based on a multi-year~~  
790 ~~climatology of Earth's shortwave radiation budget would better account for internal climate~~  
791 ~~variability in the earth system. However, CACK's flexibility regarding input year should~~  
792 ~~make it broadly appealing across a range of disciplines. One example is the land-based solar~~  
793 ~~radiation management (SRM) research community who frequently calculate from to evaluate~~  
794 ~~climate mitigation strategies.~~

795  
796 **Code and Dataset Availability**  
797 We make both monthly temporally-explicit and monthly climatological mean CACKs for  
798 years 2001-2016 available as a complete data product ("CACKv1.0"; netCDF file available at  
799 [doi:10.6073/pasta/d77b84b11be99ed4d5376d77fe0043d8](https://doi.org/10.6073/pasta/d77b84b11be99ed4d5376d77fe0043d8) DOL XXX) that includes their  
800 respective uncertainty layers. A summary of this dataset and associated variables is provided  
801 in Table S3 of the Supporting Information. A Octave-Matlab script files for generating  
802 monthly CACK with user-specified temporal and spatial extents and demonstrating its  
803 application with user-specified temporal and spatial extents is are also available at

804 DOI: [DOI.XXX](#) bundled with the netCDF file. The 2001-2016 global monthly climatological  
805 CACK provided as a Matlab data file is also available at DOI: [DOI.XXX](#).

806

## 807 Data Availability

808 CERES EBAF data are available for download at:  
809 <https://ceres.larc.nasa.gov/products.php?product=EBAF-TOA> . The CAM3 kernel is  
810 available at: <http://people.oregonstate.edu/~shellk/kernel.html> . The CAM5 kernel is  
811 available at: <https://www.earthsystemgrid.org/ac/guest/secure/sso.html> . The ECHAM5  
812 kernel is available at: [https://swiftbrowser.dkrz.de/public/dkrz\\_0c07783a-0bdc-4d5e-9f3b-c1b86fac060d/Radiative\\_kernels/](https://swiftbrowser.dkrz.de/public/dkrz_0c07783a-0bdc-4d5e-9f3b-c1b86fac060d/Radiative_kernels/) .  
813

814

## 815 Acknowledgements

816 R.M.B. was supported by the Research Council of Norway, grants #244074/E20 and  
817 #250113/F20; T.L.O. was supported by Climate and Land Use program award #2017-68002-  
818 26612 of the USDA National Institute of Food and Agriculture.

819

820

## 821 References

822 Anav, A., Friedlingstein, P., Kidston, M., Bopp, L., Caias, P., Cox, P., Jones, C., Jung, M., Myneni, R., and  
823 Zhu, Z.: Evaluating the Land and Ocean Components of the Global Carbon Cycle in the CMIP5 Earth  
824 System Models, *Journal of Climate*, 26, 6801-6843, 10.1175/JCLI-D-12-00417.1, 2013.  
825 Atwood, A. R., Wu, E., Frierson, D. M. W., Battisti, D. S., and Sachs, J. P.: Quantifying Climate Forcings  
826 and Feedbacks over the Last Millennium in the CMIP5–PMIP3 Models, *Journal of Climate*, 29, 1161-  
827 1178, 10.1175/jcli-d-15-0063.1, 2016.  
828 Block, K., and Mauritsen, T.: Forcing and feedback in the MPI-ESM-LR coupled model under abruptly  
829 quadrupled CO<sub>2</sub>, *Journal of Advances in Modeling Earth Systems*, 5, 676-691, 10.1002/jame.20041,  
830 2014.  
831 Bonan, G. B., Pollard, D., and Thompson, S. L.: Effects of Boreal Forest Vegetation on Global Climate,  
832 *Nature*, 359, 716-718, 1992.  
833 Bozzi, E., Genesio, L., Toscano, P., Pieri, M., and Miglietta, F.: Mimicking biochar-albedo feedback in  
834 complex Mediterranean agricultural landscapes, *Environmental Research Letters*, 10, 084014, 2015.  
835 Breipohl, A. M.: *Probabilistic systems analysis: an introduction to probabilistic models, decisions, and*  
836 *applications of random processes*, Wiley, New York, 1970.

837 Bretherton, C. S., Uttal, T., Fairall, C. W., Yuter, S. E., Weller, R. A., Baumgardner, D., Comstock, K.,  
838 Wood, R., and Raga, G. B.: The Epic 2001 Stratocumulus Study, *Bulletin of the American*  
839 *Meteorological Society*, 85, 967-978, 10.1175/BAMS-85-7-967, 2004.

840 Bright, R. M., and Kvælevåg, M. M.: Technical note: Evaluating a simple parameterization of radiative  
841 shortwave forcing from surface albedo change, *Atmospheric Chemistry and Physics*, 13, 11169-  
842 11174, 2013.

843 Bright, R. M.: Metrics for Biogeophysical Climate Forcings from Land Use and Land Cover Changes  
844 and Their Inclusion in Life Cycle Assessment: A Critical Review, *Environmental Science & Technology*,  
845 49, 3291-3303, 10.1021/es505465t, 2015.

846 Caiazzo, F., Malina, R., Staples, M. D., Wolfe, P., J., Yim, S. H. L., and Barrett, S. R. H.: Quantifying the  
847 climate impacts of albedo changes due to biofuel production: a comparison with biogeochemical  
848 effects, *Environmental Research Letters*, 9, 024015, 2014.

849 Carrer, D., Pique, G., Ferlicoq, M., Ceamanos, X., and Ceschia, E.: What is the potential of cropland  
850 albedo management in the fight against global warming? A case study based on the use of cover  
851 crops, *Environmental Research Letters*, 13, 044030, 2018.

852 CERES Science Team: CERES EBAF-Surface Edition 4.0. NASA Atmospheric Science and Data Center  
853 (ASDC). [https://doi.org/10.5067/TERRA+AQUA/CERES/EBAF-SURFACE\\_L3B004.0](https://doi.org/10.5067/TERRA+AQUA/CERES/EBAF-SURFACE_L3B004.0) . Accessed January  
854 14, 2018., in, 2018a.

855 CERES Science Team: CERES EBAF-TOA Edition 4.0. NASA Atmospheric Science and Data Center  
856 (ASDC). [https://doi.org/10.5067/TERRA+AQUA/CERES/EBAF-TOA\\_L3B004.0](https://doi.org/10.5067/TERRA+AQUA/CERES/EBAF-TOA_L3B004.0) . Accessed January 14,  
857 2018. , in, 2018b.

858 Cherubini, F., Bright, R. M., and Strømman, A. H.: Site-specific global warming potentials of biogenic  
859 CO<sub>2</sub> for bioenergy: contributions from carbon fluxes and albedo dynamics, *Environmental Research*  
860 *Letters*, 7, 045902, 2012.

861 Clifford, A. A.: Multivariate error analysis: A handbook of error propagation and calculation in many-  
862 parameter systems, Applied Science Publishers, London, U. K., 1973.

863 Collins, W. D., Rasch, P. J., Boville, B. A., Hack, J. J., McCaa, J. R., Williamson, D. L., Briegleb, B. P., Bitz,  
864 C. M., Lin, S.-J., and Zhang, M.: The Formulation and Atmospheric Simulation of the Community  
865 Atmosphere Model Version 3 (CAM3), *Journal of Climate*, 19, 2144-2161, 10.1175/JCLI3760.1, 2006.

866 Dickinson, R. E., and Henderson-Sellers, A.: Modelling tropical deforestation: A study of GCM land-  
867 surface parametrizations, *Quarterly Journal of the Royal Meteorological Society*, 114, 439-462,  
868 10.1002/qj.49711448009, 1988.

869 Dolinar, E. K., Dong, X., Xi, B., Jiang, J. H., and Su, H.: Evaluation of CMIP5 simulated clouds and TOA  
870 radiation budgets using NASA satellite observations, *Clim. Dyn.*, 44, 2229-2247, 10.1007/s00382-014-  
871 2158-9, 2015.

872 Donohoe, A., and Battisti, D. S.: Atmospheric and Surface Contributions to Planetary Albedo, *Journal*  
873 *of Climate*, 24, 4402-4418, 10.1175/2011JCLI3946.1, 2011.

874 Durieux, L., Machado, L. A. T., and Laurent, H.: The impact of deforestation on cloud cover over the  
875 Amazon arc of deforestation, *Remote Sensing of Environment*, 86, 132-140,  
876 [http://dx.doi.org/10.1016/S0034-4257\(03\)00095-6](http://dx.doi.org/10.1016/S0034-4257(03)00095-6), 2003.

877 Free, M., and Sun, B.: Trends in U.S. Total Cloud Cover from a Homogeneity-Adjusted Dataset,  
878 *Journal of Climate*, 27, 4959-4969, 10.1175/jcli-d-13-00722.1, 2014.

879 Gao, F., He, T., Wang, Z., Ghimire, B., Shuai, Y., Masek, J., Schaaf, C., and Williams, C.: Multi-scale  
880 climatological albedo look-up maps derived from MODIS BRDF/albedo products, *Journal of Applied*  
881 *Remote Sensing*, 8, 2014.

882 Ghimire, B., Williams, C. A., Masek, J., Gao, F., Wang, Z., Schaaf, C., and He, T.: Global albedo change  
883 and radiative cooling from anthropogenic land cover change, 1700 to 2005 based on MODIS, land use  
884 harmonization, radiative kernels, and reanalysis, *Geophysical Research Letters*, 41, 9087-9096,  
885 10.1002/2014GL061671, 2014.

886 Green, P., Gardiner, T., Medland, D., and Cimini, D.: WP2: Guide to uncertainty in measurement and  
887 its nomenclature. Version 4.0. , U.K., 212, 2017.

888 Hurrell, J. W., Holland, M. M., Gent, P. R., Ghan, S., Kay, J. E., Kushner, P. J., Lamarque, J. F., Large, W.  
889 G., Lawrence, D., Lindsay, K., Lipscomb, W. H., Long, M. C., Mahowald, N., Marsh, D. R., Neale, R. B.,  
890 Rasch, P., Vavrus, S., Vertenstein, M., Bader, D., Collins, W. D., Hack, J. J., Kiehl, J., and Marshall, S.:  
891 The Community Earth System Model: A Framework for Collaborative Research, *Bulletin of the*  
892 *American Meteorological Society*, 94, 1339-1360, 10.1175/BAMS-D-12-00121.1, 2013.  
893 Iqbal, M.: An introduction to solar radiation, Academic Press Canada, Ontario, CA, 389 pp., 1983.  
894 Jones, A. D., Calvin, K. V., Collins, W. D., and Edmonds, J.: Accounting for radiative forcing from  
895 albedo change in future global land-use scenarios, *Climatic Change*, 131, 691-703, 10.1007/s10584-  
896 015-1411-5, 2015.  
897 Kashimura, H., Abe, M., Watanabe, S., Sekiya, T., Ji, D., Moore, J. C., Cole, J. N. S., and Kravitz, B.:  
898 Shortwave radiative forcing, rapid adjustment, and feedback to the surface by sulfate  
899 geoengineering: analysis of the Geoengineering Model Intercomparison Project G4 scenario, *Atmos.*  
900 *Chem. Phys.*, 17, 3339-3356, 2017.  
901 Kato, S., Loeb, N. G., Rose, F. G., Doelling, D. R., Rutan, D. A., Caldwell, T. E., Yu, L., and Weller, R. A.:  
902 Surface Irradiances Consistent with CERES-Derived Top-of-Atmosphere Shortwave and Longwave  
903 Irradiances, *Journal of Climate*, 26, 2719-2740, 10.1175/JCLI-D-12-00436.1, 2012.  
904 Kato, S., Loeb, N. G., Rose, F. G., Doelling, D. R., Rutan, D. A., Caldwell, T. E., Yu, L., and Weller, R. A.:  
905 Surface irradiances consistent with CERES-derived top-of-atmosphere shortwave and longwave  
906 irradiances, *Journal of Climate*, 26, 2719-2740, 2013.  
907 Kato, S., Rose, F. G., Rutan, D. A., Thorsen, T. J., Loeb, N. G., Doelling, D. R., Huang, X., Smith, W. L.,  
908 Su, W., and Ham, S.-H.: Surface Irradiances of Edition 4.0 Clouds and the Earth's Radiant Energy  
909 System (CERES) Energy Balanced and Filled (EBAF) Data Product, *Journal of Climate*, 31, 4501-4527,  
910 10.1175/JCLI-D-17-0523.1, 2018.  
911 Lacis, A. A., and Hansen, J. E.: A parameterization for the absorption of solar radiation in the earth's  
912 atmosphere, *Journal of Atmospheric Sciences*, 31, 118-133, 1974.  
913 Lawrence, D., and Vandecar, K.: Effects of tropical deforestation on climate and agriculture, *Nature*  
914 *Climate Change*, 5, 27, 10.1038/nclimate2430  
915 <https://www.nature.com/articles/nclimate2430#supplementary-information>, 2014.  
916 Lenton, T. M., and Vaughan, N. E.: The radiative forcing potential of different climate geoengineering  
917 options, *Atmospheric Chemistry and Physics* 9, 5539-5561, 2009.  
918 Li, J. L. F., Waliser, D. E., Stephens, G., Lee, S., L'Ecuyer, T., Kato, S., Loeb, N., and Ma, H.-Y.:  
919 Characterizing and understanding radiation budget biases in CMIP3/CMIP5 GCMs, contemporary  
920 GCM, and reanalysis, *Journal of Geophysical Research: Atmospheres*, 118, 8166-8184,  
921 10.1002/jgrd.50378, 2013.  
922 Loeb, N. G., Wielicki, B. A., Doelling, D. R., Smith, G. L., Keyes, D. F., Kato, S., Manalo-Smith, N., and  
923 Wong, T.: Toward optimal closure of the Earth's top-of-atmosphere radiation budget, *Journal of*  
924 *Climate*, 22, 748-766, 2009.  
925 Loeb, N. G., Doelling, D. R., Wang, H., Su, W., Nguyen, C., Corbett, J. G., Liang, L., Mitrescu, C., Rose, F.  
926 G., and Kato, S.: Clouds and the Earth's Radiant Energy System (CERES) Energy Balanced and Filled  
927 (EBAF) Top-of-Atmosphere (TOA) Edition-4.0 Data Product, *Journal of Climate*, 31, 895-918,  
928 10.1175/JCLI-D-17-0208.1, 2017.  
929 Lutz, D. A., Burakowski, E. A., Murphy, M. B., Borsuk, M. E., Niemic, R. M., and Howarth, R. B.:  
930 Tradeoffs between three forest ecosystem services across the state of New Hampshire, USA: timber,  
931 carbon, and albedo, *Ecological Applications*, 26, 146-161, 10.1890/14-2207.1, 2015.  
932 Lutz, D. A., and Howarth, R. B.: The price of snow: albedo valuation and a case study for forest  
933 management, *Environmental Research Letters*, 10, 064013, 2015.  
934 Mahadevan, S., and Sarkar, S.: Uncertainty analysis methods, U.S. Department of Energy,  
935 Washington, D.C., USA, 32, 2009.  
936 Muñoz, I., Campra, P., and Fernández-Alba, A. R.: Including CO<sub>2</sub>-emission equivalence of changes in  
937 land surface albedo in life cycle assessment. Methodology and case study on greenhouse agriculture,  
938 *International Journal of Life Cycle Assessment*, 15, 672-681, 2010.

939 O'Halloran, T. L., Law, B. E., Goulden, M. L., Wang, Z., Barr, J. G., Schaaf, C., Brown, M., Fuentes, J. D.,  
940 Göckede, M., Black, A., and Engel, V.: Radiative forcing of natural forest disturbances, *Global Change  
941 Biology*, 18, 555-565, 2012.

942 Pendergrass, A. G., Conley, A., and Vitt, F. M.: Surface and top-of-atmosphere radiative feedback  
943 kernels for CESM-CAM5, *Earth Syst. Sci. Data*, 10, 317-324, 10.5194/essd-10-317-2018, 2018.

944 Qu, X., and Hall, A.: Assessing Snow Albedo Feedback in Simulated Climate Change, *Journal of  
945 Climate*, 19, 2617-2630, 10.1175/JCLI3750.1, 2006.

946 Randerson, J. T., Liu, H., Flanner, M. G., Chambers, S. D., Jin, Y., Hess, P. G., Pfister, G., Mack, M. C.,  
947 Treseder, K. K., Welp, L. R., Chapin, F. S., Harden, J. W., Goulden, M. L., Lyons, E., Neff, J. C., Schuur, E.  
948 A. G., and Zender, C. S.: The Impact of Boreal Forest Fire on Climate Warming, *Science*, 314, 1130-  
949 1132, 2006.

950 Rasool, S. I., and Schneider, S. H.: Atmospheric Carbon Dioxide and Aerosols: Effects of Large  
951 Increases on Global Climate, *Science*, 173, 138-141, 10.1126/science.173.3992.138, 1971.

952 Richter, I.: Climate model biases in the eastern tropical oceans: causes, impacts and ways forward,  
953 *Wiley Interdisciplinary Reviews: Climate Change*, 6, 345-358, 10.1002/wcc.338, 2015.

954 Schmidt, M., and Lipson, H.: Distilling free-form natural laws from experimental data, *science*, 324,  
955 81-85, 2009.

956 Schmidt, M., and Lipson, H.: Symbolic regression of implicit equations, in: *Genetic Programming  
957 Theory and Practice VII*, Springer, 73-85, 2010.

958 Shell, K. M., Kiehl, J. T., and Shields, C. A.: Using the Radiative Kernel Technique to Calculate Climate  
959 Feedbacks in NCAR's Community Atmospheric Model, *Journal of Climate*, 21, 2269-2282,  
960 10.1175/2007JCLI2044.1, 2008.

961 Smits, G. F., and Kotanchek, M.: Pareto-front exploitation in symbolic regression, in: *Genetic  
962 programming theory and practice II*, Springer, 283-299, 2005.

963 Soden, B. J., Held, I. M., Colman, R., Shell, K. M., Kiehl, J. T., and Shields, C. A.: Quantifying climate  
964 feedbacks using radiative kernels, *Journal of Climate*, 21, 3504-3520, Doi 10.1175/2007jcli2110.1,  
965 2008.

966 Srivastava, R.: Trends in aerosol optical properties over South Asia, *International Journal of  
967 Climatology*, 37, 371-380, doi:10.1002/joc.4710, 2017.

968 Stephens, G. L., O'Brien, D., Webster, P. J., Pilewski, P., Kato, S., and Li, J.-I.: The albedo of Earth,  
969 *Reviews of Geophysics*, 53, 141-163, 10.1002/2014RG000449, 2015.

970 Stevens, B., Giorgetta, M., Esch, M., Mauritsen, T., Crueger, T., Rast, S., Salzmann, M., Schmidt, H.,  
971 Bader, J., Block, K., Brokopf, R., Fast, I., Kinne, S., Kornblueh, L., Lohmann, U., Pincus, R., Reichler, T.,  
972 and Roeckner, E.: Atmospheric component of the MPI-M Earth System Model: ECHAM6, *Journal of  
973 Advances in Modeling Earth Systems*, 5, 146-172, doi:10.1002/jame.20015, 2013.

974 Taylor, K. E., Crucifix, M., Braconnot, P., Hewitt, C. D., Doutriaux, C., Broccoli, A. J., Mitchell, J. F. B.,  
975 and Webb, M. J.: Estimating Shortwave Radiative Forcing and Response in Climate Models, *Journal of  
976 Climate*, 20, 2530-2543, 10.1175/JCLI4143.1, 2007.

977 The GFDL Global Atmospheric Model Development Team: The New GFDL Global Atmosphere and  
978 Land Model AM2-LM2: Evaluation with Prescribed SST Simulations, *Journal of Climate*, 17, 4641-  
979 4673, 10.1175/JCLI-3223.1, 2004.

980 Vanderhoof, M., Williams, C. A., Ghimire, B., and Rogan, J.: Impact of mountain pine beetle outbreaks  
981 on forest albedo and radiative forcing, as derived from Moderate Resolution Imaging  
982 Spectroradiometer, Rocky Mountains, USA, *Journal of Geophysical Research: Biogeosciences*, 118,  
983 1461-1471, 10.1002/jgrg.20120, 2013.

984 Wang, H., and Su, W.: Evaluating and understanding top of the atmosphere cloud radiative effects in  
985 Intergovernmental Panel on Climate Change (IPCC) Fifth Assessment Report (AR5) Coupled Model  
986 Intercomparison Project Phase 5 (CMIP5) models using satellite observations, *Journal of Geophysical  
987 Research: Atmospheres*, 118, 683-699, doi:10.1029/2012JD018619, 2013.

988 Winton, M.: Simple optical models for diagnosing surface-atmosphere shortwave interactions,  
989 *Journal of Climate*, 18, 3796-3806, 2005.

990 Winton, M.: Surface Albedo Feedback Estimates for the AR4 Climate Models, *Journal of Climate*, 19,  
991 359-365, 10.1175/jcli3624.1, 2006.  
992 Wright, J. S., Fu, R., Worden, J. R., Chakraborty, S., Clinton, N. E., Risi, C., Sun, Y., and Yin, L.:  
993 Rainforest-initiated wet season onset over the southern Amazon, *Proceedings of the National  
994 Academy of Sciences*, 201621516, 10.1073/pnas.1621516114, 2017.  
995 Zhao, D., Xin, J., Gong, C., Wang, X., Ma, Y., and Ma, Y.: Trends of Aerosol Optical Properties over the  
996 Heavy Industrial Zone of Northeastern Asia in the Past Decade (2004–15), *Journal of the Atmospheric  
997 Sciences*, 75, 1741-1754, 10.1175/jas-d-17-0260.1, 2018.

998

999 **Table 1.** Attributes of existing GCM kernels, all of which having a monthly temporal  
1000 resolution.

<u>Kernel</u>	<u>Base climatology extent</u>	<u>Base climatology period</u>	<u>Shortwave Radiative transfer</u>	<u>Horizontal Resolution</u>	<u>References</u>
<u>ECHAM6</u>	<u>1,000 years</u>	<u>Preindustrial*</u>	<u>RRTM-G</u>	<u><math>1.88^\circ \times 1.88^\circ</math></u>	<u>(Block and Mauritsen, 2014; Stevens et al., 2013)</u>
<u>CAM3</u>	<u>6 years</u>	<u>1995-2000</u>	<u><math>\delta</math>-Eddington</u>	<u><math>1.4^\circ \times 1.4^\circ</math></u>	<u>(Shell et al., 2008; Collins et al., 2006)</u>
<u>CAM5</u>	<u>1 year</u>	<u>2006-2007</u>	<u>RRTM-G</u>	<u><math>0.94^\circ \times 1.25^\circ</math></u>	<u>(Pendergrass et al., 2018)</u>
<u>GFDL</u>	<u>17 years</u>	<u>1979-1995</u>	<u>Exponential sum-fits, 18 bands</u>	<u><math>2^\circ \times 2.5^\circ</math></u>	<u>(Soden et al., 2008; The GFDL Global Atmospheric Model Development Team, 2004)</u>

1001 \*Atmospheric CO<sub>2</sub> concentration = 284.7 ppmv; Exact time period unknown

1004 **Table 12.** Definition of CERES input variables and other system optical properties derived  
 1005 from CERES inputs. All variables [are have a 2001–2016 monthly means monthly temporal](#)  
 1006 [resolution and a at 1° × 1° spatial resolution of 1° × 1°.](#)

#### CERES EBAF v.4 Shortwave Boundary Fluxes

$SW_{\downarrow}^{TOA}$	Downwelling solar flux at top-of-atmosphere	$\text{Wm}^{-2}$
$SW_{\downarrow}^{SFC}$	Downwelling solar flux at surface	$\text{Wm}^{-2}$
$SW_{\downarrow,CLR}^{SFC}$	Clear-sky downwelling solar flux at surface	$\text{Wm}^{-2}$
$SW_{\uparrow}^{TOA}$	Upwelling solar flux at top-of-atmosphere	$\text{Wm}^{-2}$
$SW_{\uparrow}^{SFC}$	Upwelling solar flux at surface	$\text{Wm}^{-2}$

#### System Optical Properties

$T = SW_{\downarrow}^{SFC} / SW_{\downarrow}^{TOA}$	Clearness index	unitless
$\alpha_p = SW_{\uparrow}^{TOA} / SW_{\downarrow}^{TOA}$	Planetary albedo	unitless
$\alpha_s = SW_{\uparrow}^{SFC} / SW_{\downarrow}^{SFC}$	Surface albedo	unitless
$A_p = 1 - \alpha_p$	Effective planetary absorption	unitless
$A_s = [SW_{\downarrow}^{SFC} - SW_{\uparrow}^{SFC}] / SW_{\downarrow}^{TOA}$	Effective surface absorption	unitless
$A_a = A_p - A_s$	Effective atmospheric absorption	unitless
$T_a = 1 - A_a$	Effective atmospheric transmission	unitless
$T_{a,CLR} = 1 - A_{a,CLR}$	Clear-sky effective atmospheric transmission	unitless
$\tau$	Cloud visible optical depth	unitless
$c$	Cloud area fraction	fraction

1007

1008

1009 **Table 23.** Normalized absolute deviation and CERES kernel [model candidate](#) ranking.

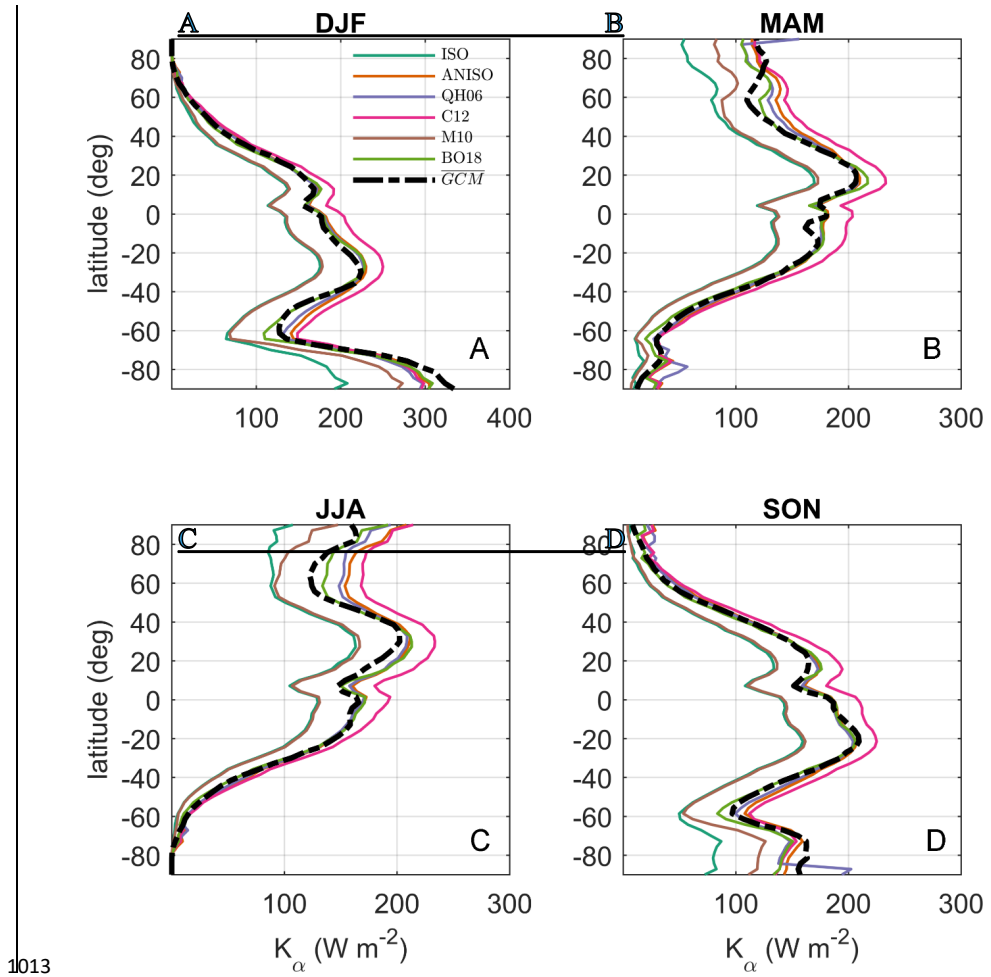
	<b>Global</b>		<b>Land only</b>		Mean Rank
	$\overline{NAD}$	Rank	$\overline{NAD}$	Rank	
<b>ISO</b>	0.05	6	0.05	6	6
<b>ANISO</b>	0.64	3	0.59	3	3
<b>C12</b>	0.45	4	0.47	4	4
<b>M10</b>	0.26	5	0.34	5	5
<b>QH06</b>	0.66	2	0.60	2	2
<b>BO18</b>	0.67	1	0.64	1	1

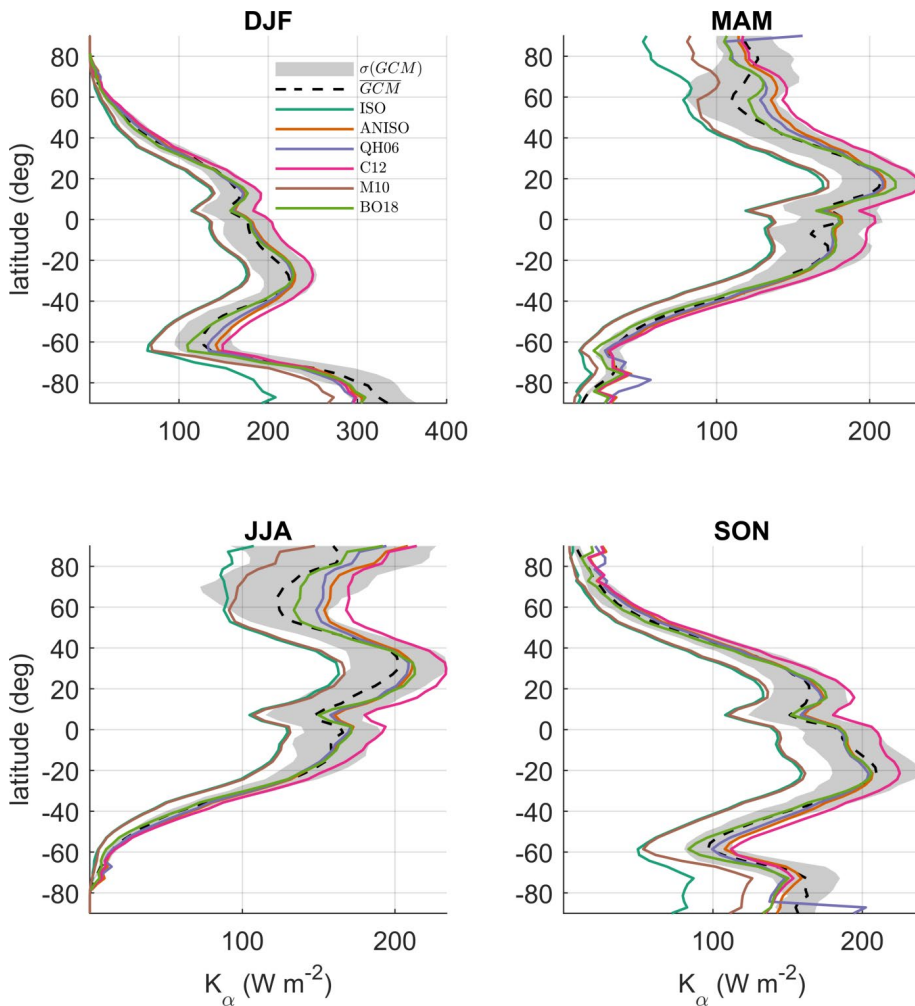
1010

1011

**Table 34.** Global monthly mean bias ( $MB$ ) and mean absolute bias ( $MAB$ ) for  $K_{\alpha}^{BO18}$  emulated with  $T$  and  $SW_{\downarrow}^{SFC}$  from ECHAM6 and CAM5. For reference, the global mean value of  $K_{\alpha}^{BO18}$  is  $133 \text{ W m}^{-2}$ .

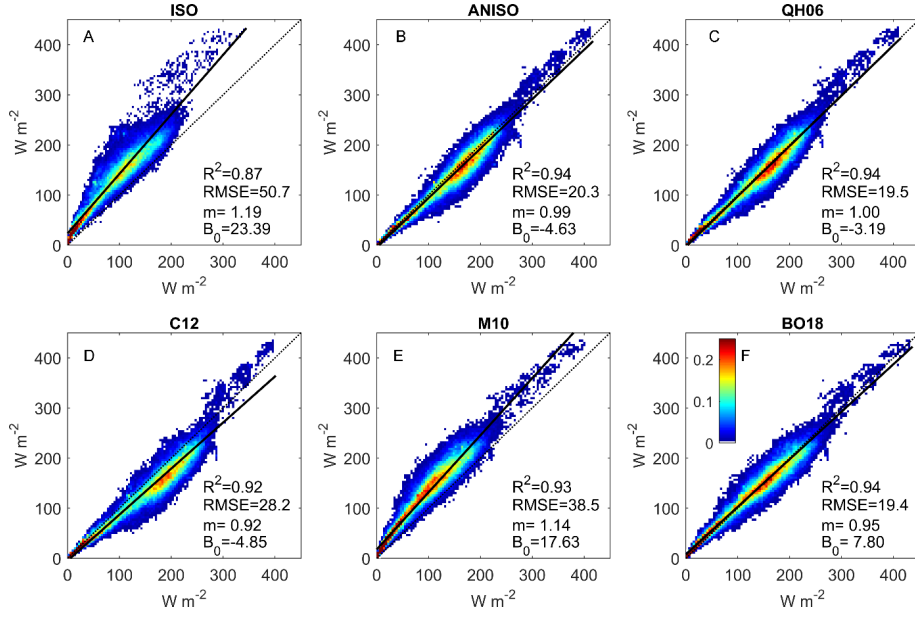
	$MB (\text{W m}^{-2})$												
	Jan.	Feb.	Mar.	Apr.	May	Jun.	Jul.	Aug.	Sep.	Oct.	Nov.	Dec.	Ann.
$K_{\alpha}^{BO18} - K_{\alpha}^{CAM5}$	-2.9	-3.4	-3.3	-3.9	-4.4	-3.8	-3.8	-3.7	-3.4	-3.8	-3.7	-3.3	-3.6
$K_{\alpha}^{BO18} - K_{\alpha}^{ECHAM6}$	-1.9	-2.2	-1.8	-1.9	-2.2	-1.5	-1.1	-1.6	-1.7	-2.5	-2.5	-1.8	-1.9
	$MAB (\text{W m}^{-2})$												
	Jan.	Feb.	Mar.	Apr.	May	Jun.	Jul.	Aug.	Sep.	Oct.	Nov.	Dec.	Ann.
$ K_{\alpha}^{BO18} - K_{\alpha}^{CAM5} $	6.9	5.7	5.2	6.8	7.7	8.6	7.9	6.7	5.6	6.1	6.9	6.9	6.8
$ K_{\alpha}^{BO18} - K_{\alpha}^{ECHAM6} $	6.3	5.7	5.0	5.9	6.7	6.8	6.4	5.8	5.3	5.6	6.4	6.7	6.1



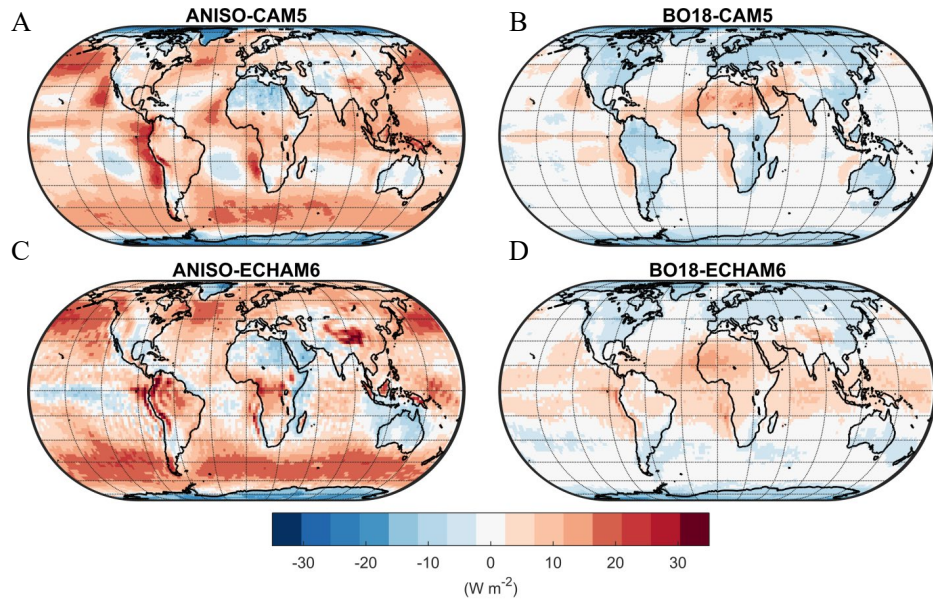


1014 **Figure 1.** Latitudinal (1°) and seasonal means of the multi-GCM mean ( $K_\alpha^{\text{GCM}}$ ) and CACK  
 1015  $K_\alpha^{\text{CERES}}$  model candidates for: A) December-January-February (DJF); B) March-April-May  
 1016 (MAM); C) June-July-August (JJA); D) September-October-November (SON).

1018



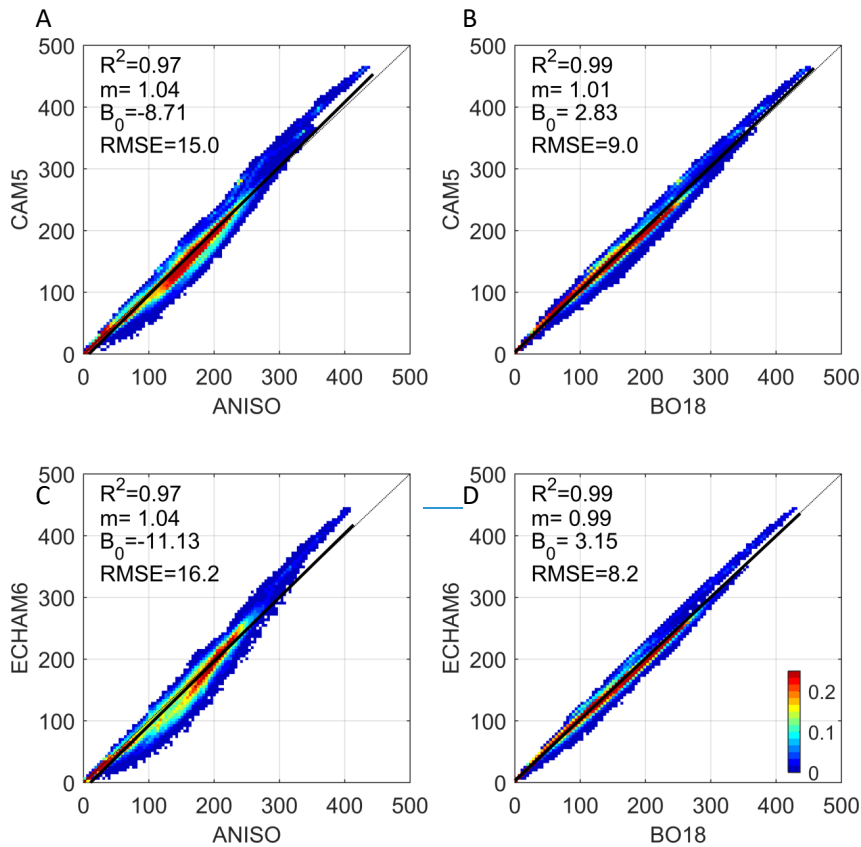
1019 **Figure 2.** A)-F): Scatter-density regressions of global monthly mean  $K_\alpha^{\text{GCM}}$  (y-axis) and  
1020  $K_\alpha^{\text{CERES}}$  (x-axis), with the CERES kernel identifier shown at the top of each sub-panel. “ $m$ ” =  
1021 slope; “ $B_0$ ” = y-intercept. [The color scale indicates the percentage of regression points that](#)  
1022 [fall within an averaging bin, where the x-axis and y-axis have been gridded into  \$100 \times 100\$](#)   
1023 [equally-spaced bins to help illustrate the density of overlapping points. The color scale](#)  
1024 [indicates the percentage of regression points that fall within a  \$100 \times 100\$  sample grid centered](#)  
1025 [on the plotted point.](#)



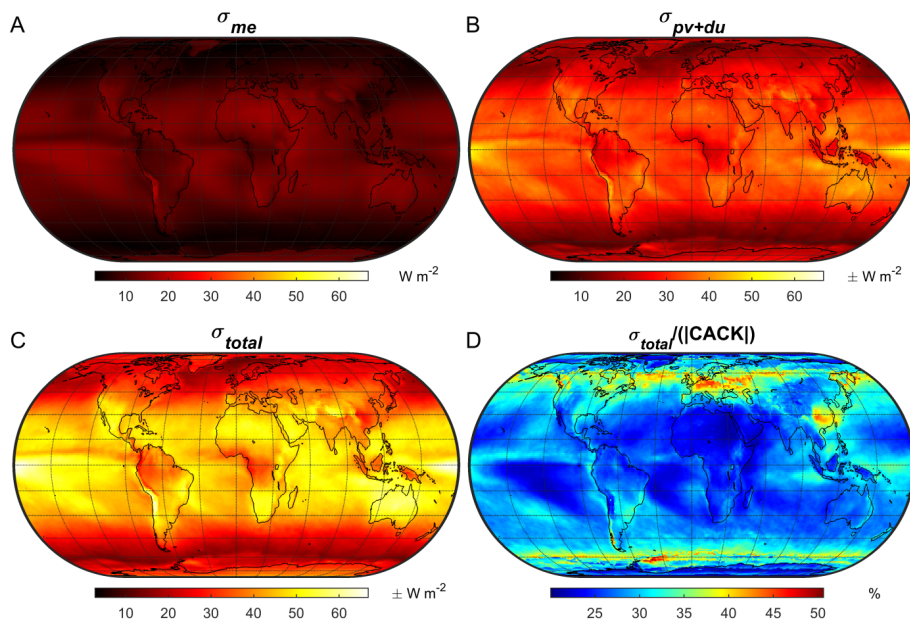
1028

1029 **Figure 3.** A) Mean annual bias of the CAM5 albedo change kernel emulated with the ANISO  
 1030 analytical\_semi-empirical model; B) Mean annual bias of the CAM5 albedo change kernel  
 1031 emulated with the BO18 parameterization; C) Mean annual bias of the ECHAM6 albedo  
 1032 change kernel emulated with the ANISO semi-empiricalanalytical model; D) Mean annual  
 1033 bias of the ECHAM6 albedo change kernel emulated with the BO18 parameterization

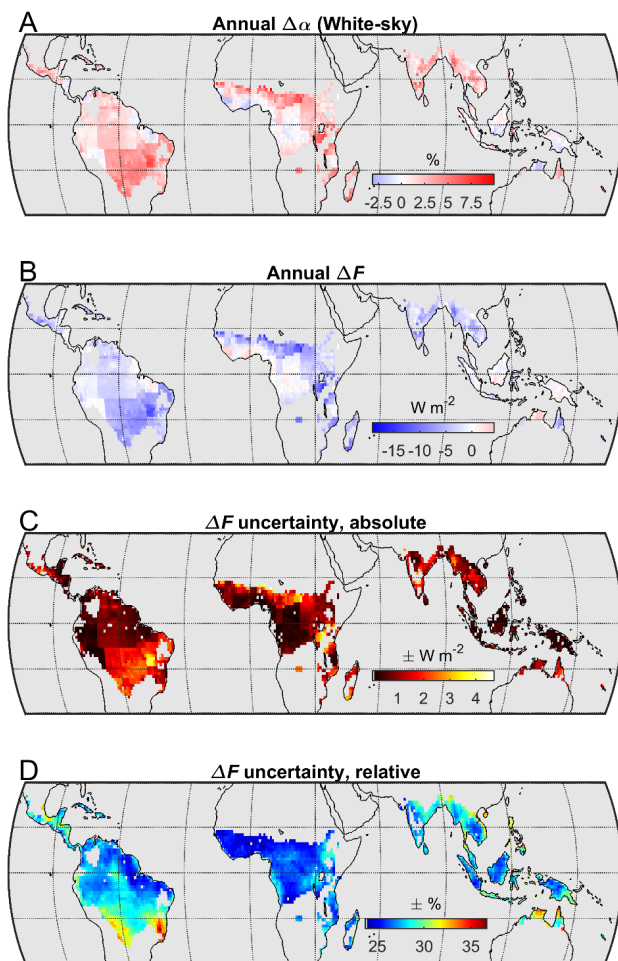
1034



1035 **Figure 4.** A)-D): Scatter-density regressions of  $K_{\alpha}^{GCM}$  (y-axis) and  $K_{\alpha}^{GCM}$  emulated with the  
 1036 ANISO [semi-empirical](#) model and BO18 parameterization (x-axis); “ $m$ ” = slope; “ $B_0$ ” = y-  
 1037 intercept. [The color scale indicates the percentage of regression points that fall within a 100 ×](#)  
 1038 [100 sample grid centered on the plotted point. See Figure 2 caption for a description of the](#)  
 1039 [color scale.](#)



1043 **Figure 5.** Annual uncertainty of a CACK based on 2001-2016 monthly mean CERES EBAF  
 1044 v4 climatology: A) The absolute uncertainty related to *model error* (i.e., the  $K_{\alpha_s}^{BO18}$   
 1045 parameterization); B) The total propagated absolute uncertainty related to *physical variability*  
 1046 and *data uncertainty* of CACK input variables; C) Total absolute uncertainty; D) Total  
 1047 relative uncertainty.  
 1048  
 1049



1050  
1051 [Figure 6. Example application of a CACK based on the 2001-2016 monthly mean CERES](#)  
1052 [EBAF v4 climatology. A\) Annual mean of the climatological \(i.e., 2001-2011\) monthly](#)  
1053 [mean difference in white-sky surface albedo between grasslands and evergreen broadleaved](#)  
1054 [forests \( \$\Delta\alpha\_s\$ \) based on the 1° product of Gao \*et al.\* \(2014\); B\) Annual mean instantaneous](#)  
1055 [radiative forcing \( \$\Delta F\$ \) of monthly mean  \$\Delta\alpha\_s\$  estimated with CACK; C\) Absolute uncertainty](#)

Field Code Changed

Field Code Changed

Field Code Changed

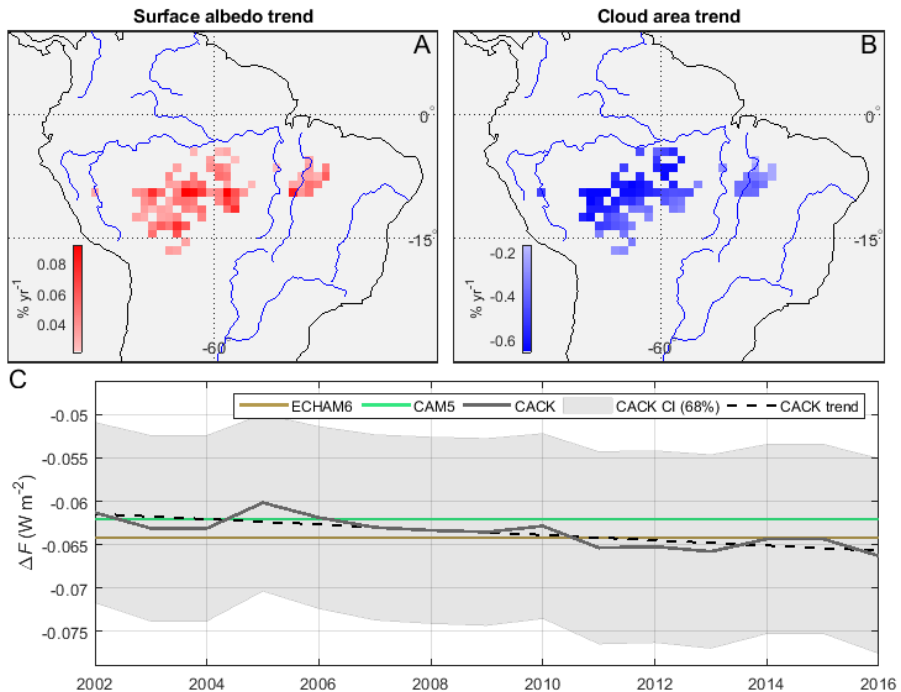
1056 (annual mean) of the CACK-based  $\Delta F$  estimate, including the uncertainty of  $\Delta\alpha_s$  (D)

Field Code Changed

Field Code Changed

1057 Relative uncertainty (annual mean) of the CACK-based  $\Delta F$  estimate.

Field Code Changed



1058 **Figure 7.** Example application of a temporally-explicit CACK. A) 2001-2016 statistically  
 1059 significant positive trends in all-sky *surface albedo* derived from CERES EBAF-Surface v4;  
 1060 B) 2001-2016 statistically significant negative trends in *cloud area* derived from CERES  
 1061 EBAF-TOA v4; C) Mean local  $\Delta F$  from  $\Delta \alpha_s$  when estimated with the CACK, ECHAM6,  
 1062 and CAM5 surface albedo change kernels. The  $1\sigma$  confidence interval (“CI”) shown for  
 1063 CACK excludes the uncertainty component related to *physical variability*.  
 1064

Field Code Changed  
 Field Code Changed